PERFORMANCE/COST RANGE ANALYSIS TECHNICAL REPORT

ADVANCED TECHNOLOGY DEVELOPMENT FOR MISSILE GRADE LASER GYROS

(CONTRACT N00123-78-C-0821
ITEM 0002, SEQ. NO. A003)

Feb 80

Prepared for
NAVAL WEAPONS CENTER
CHINA LAKE, CA. 93555

SPERRY

SG-4224-1169

GREAT NECK, NEW YORK 11020

REPORT DOCUMENTATION PAGE

1a. REPORT SECURITY CLASSIFICATION: UNCLASSIFIED	1b. RESTRICTIVE MARKINGS
2a. SECURITY CLASSIFICATION AUTHORITY	3. DISTRIBUTION/AVAILABILITY OF REPORT: Unlimited
2b. DECLASSIFICATION/DOWNGRADING SCHEDULE	
4. PERFORMING ORGANIZATION REPORT NUMBER(S): SG-4224-1169	5. MONITORING ORGANIZATION REPORT NUMBER(S)
6a. NAME OF PERFORMING ORGANIZATION: Sperry; 6b. OFFICE SYMBOL (If applicable)	7a. NAME OF MONITORING ORGANIZATION: Naval Weapons Center
6c. ADDRESS (City, State, and ZIP Code): Great Neck, NY 11020	7b. ADDRESS (City, State, and ZIP Code): China Lake, CA 93555
8a. NAME OF FUNDING/SPONSORING ORGANIZATION: Naval Weapons Center; 8b. OFFICE SYMBOL (If applicable)	9. PROCUREMENT INSTRUMENT IDENTIFICATION NUMBER: N00123-78-C-0821
8c. ADDRESS (City, State, and ZIP Code): China Lake, CA 93555	10. SOURCE OF FUNDING NUMBERS: PROGRAM ELEMENT NO. / PROJECT NO. / TASK NO. / WORK UNIT ACCESSION NO.

11. TITLE (Include Security Classification): Advanced Technology Development for Missile Grade Laser Gyros

12. PERSONAL AUTHOR(S)

13a. TYPE OF REPORT	13b. TIME COVERED	14. DATE OF REPORT (Year, Month, Day)	15. PAGE COUNT
Final	FROM _____ TO _____	Feb. 1980	70

16. SUPPLEMENTARY NOTATION

17. COSATI CODES			18. SUBJECT TERMS (Continue on reverse if necessary and identify by block number)
FIELD	GROUP	SUB-GROUP	Laser Gyro Inertial Sensor
17	07		

19. ABSTRACT (Continue on reverse if necessary and identify by block number)

An analysis was conducted of the performance/cost range potential for the Sperry Model SLIC-7 baseline gyro design. Consideration was given to cost reduction and performance improvement features that could be incorporated in order to respond to the broadest possible spectrum of future guidance system requirements.

20. DISTRIBUTION/AVAILABILITY OF ABSTRACT: ☐ UNCLASSIFIED/UNLIMITED ☐ SAME AS RPT ☒ DTIC USERS	21. ABSTRACT SECURITY CLASSIFICATION: UNCLASSIFIED
22a. NAME OF RESPONSIBLE INDIVIDUAL: A.S. Glista	22b. TELEPHONE (Include Area Code): (202) 692-2515; 22c. OFFICE SYMBOL: AIR-933E

PERFORMANCE/COST RANGE ANALYSIS TECHNICAL REPORT

ADVANCED TECHNOLOGY DEVELOPMENT FOR MISSILE GRADE LASER GYROS

(CONTRACT N00123-78-C-0821
ITEM 0002, SEQ. NO. A003)

Prepared for
NAVAL WEAPONS CENTER
CHINA LAKE, CA. 93555

SPERRY
GREAT NECK, NEW YORK 11020

SG-4224-1169
FEBRUARY 1980

TABLE OF CONTENTS

LIST OF ILLUSTRATIONS

Section 1

INTRODUCTION AND SUMMARY

1.1 INTRODUCTION

This performance/cost range analysis technical report has been prepared in accordance with Naval Weapons Center contract number N00123-78-C-0821 Statement of Work (SOW). This report is submitted to fulfill the contract data item A003 - Technical Report (Performance/Cost Range Analysis).

1.1.1 Requirements

The requirements for the report and its objectives are described in the following SOW excerpt:

> f. "Conduct an analysis of the performance/cost range potential for the baseline gyro design. Consider cost reducing and/or performance improving features that could be incorporated into the baseline design to respond to the broadest possible spectrum of future guidance system requirements. Limit design changes to no change in lasing frequency, no change in lock-in circumvention technique, no radical block geometry changes (other than scaling larger or smaller), and no change in mirror coatings. Develop cost targets in constant FY '78 dollars for the baseline gyro (recurring production costs only). Analyze design variants and calculate cost and performance impact. Deliver an analysis report."

The performance spectrum to be addressed was established in the SOW and duplicated in table 1-1. The three key strapdown laser gyro performance parameters associated with inertial guidance system requirements are:

Bias uncertainty °/HR

Random drift $°/\sqrt{HR}$

Scale factor error PPM

This report addresses the specified range of performance for these parameters and presents derivatives of the baseline laser gyro that satisfy both ends of the spectrum. The production costs for these sensors are estimated based on 1978 dollars and a production run of 2000 axes at 100 axes per month.

1.1.2 Baseline Laser Gyro

The baseline laser gyro is the Sperry Model SLIC-7 three-axis triad which consists of two separate assemblies: a sensor assembly part number 6077074 and an electronics assembly part number 6077072. Figure 1-1 is a photograph of these assemblies. The sensor assembly, a cylinder measuring 4.25 inches in diameter by 5.4 inches long, houses three 7.5-inch perimeter laser gyros. These three gyros have their optical paths interwoven on a common low thermal expansion block to minimize cost and size. The laser gyros are modularly constructed, that is all optical assemblies "plug into" the common block, as a further step towards minimizing production costs.

The generic baseline design is triangular and employs a magneto-optic corner mirror to circumvent the rate threshold inherent in all laser gyros. The lasing medium is a helium-neon gas discharge that operates in the near infrared (1.15 micron transition).

The electronics assembly contains hybrid electronics (to minimize size) that provide the closed loop control necessary for proper gyro operation. These electronics are designed to satisfy the total range of performance requirements and are, therefore, a constant factor in the performance/cost range analysis. (That is, the same electronics are used with all sensor configurations.)

Table 1-1 tabulates the characteristics of the baseline gyro against the specification range. As can be seen, the SLIC-7 is about mid-range.

1.2 SUMMARY OF RESULTS

As stated above, the objective of this analysis was to configure alternate laser gyro configurations that could satisfy the entire performance spectrum. The basic

Table 1-1. Missile Grade Laser Gyro Performance Requirements

Parameter	Specification		SLIC 7
Gyro Performance Range (28 VDC in, pulses out, single axis gyro)	Hi Performance Application	Lo Performance Application	Baseline Gyro
Cost goal, 1978 constant dollars, average for first production run of 2000 units, recurring costs only	$6,000 ea	$1,500 ea	$4,238 ea
Bias uncertainty, all causes, long term, degrees/hours, 1σ	0.02	3.0	0.5
Random drift, degrees/$\sqrt{\text{hr}}$, 1σ	0.005	1.0	0.05
Scale factor, radians per pulse	2^{-16}	2^{-14}	2^{-16}
Input axis alignment, milliradians	1.0	2.0	0.1
Input axis stability, microradians, 1σ	±75	±500	±100
Scale factor error, all causes, ppm	20	500	100
Rate capability, degrees/sec	±400	±800	±800
Weight, maximum, lbs	6.0	3.0	3.2
Volume, maximum, cu. in.	100	70	47

task ground rule was that the generic design must be retained per the instructions in the SOW. This ground rule essentially dictates that the only parameter available to trade-off versus performance is the optical path geometry. Therefore, performance dependence on geometry had to be established.

The generic triangular design was retained so that all performance scaling laws are based on perimeter length (longer perimeter, better performance).

The scaling laws documented in section 3.2 establish the relationship of performance to perimeter for the generic configuration. In general a theoretical treatise is presented with the resulting relationship validated (section 3.3) against

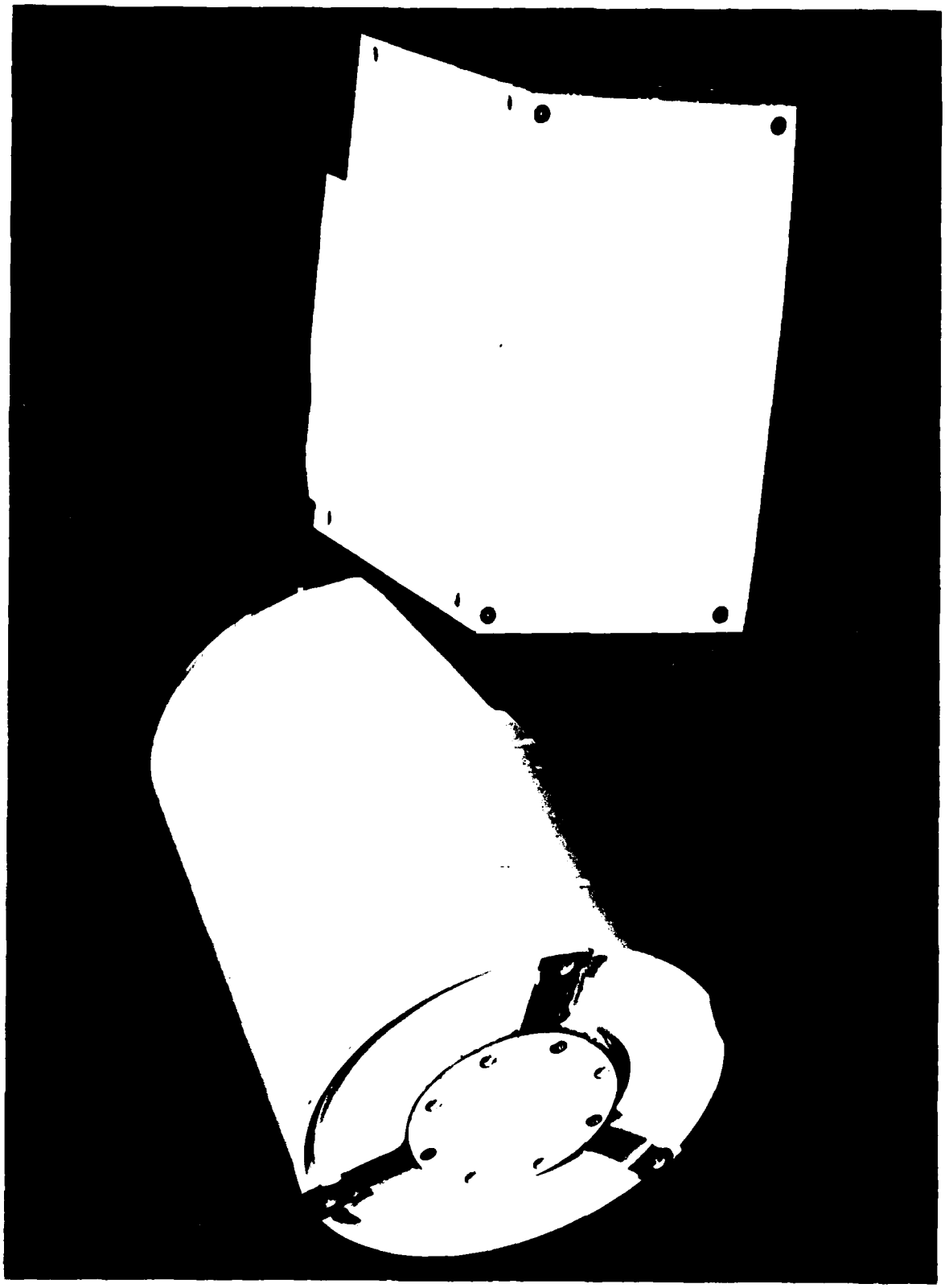

Figure 1-1. Baseline Laser Gyro - Sperry SLIC 7

empirical data obtained on the family of Sperry laser gyros (7.5, 15 and 21 inch perimeters). These laws were then applied to the "mid range" baseline gyro performance characteristics (drift uncertainty, random drift and scale factor error) to establish a gyro size to satisfy the high performance end of the range. To satisfy the low end, a simplified SLIC-7 is used in lieu of a smaller gyro because of the size constraint imposed by the use of a modular design (discharge length restricted to a single leg of the optical path).

The production cost for each of the three configurations was then estimated. The SLIC-7 baseline gyro was used to establish a baseline production cost (detailed in Appendix A). Sperry has been building the SLIC-7 for several years and, therefore, has the background to establish meaningful estimates for this sensor. To date, 12 of these units have been built with 10 currently going through a build cycle. An aggressive design-to-cost effort has resulted in significant cost reducing changes over the past year.

The results of the performance/cost range analysis are summarized in tabular form in table 1-2. To provide insight into intermediate requirements, figures 1-2 and 1-3 are presented. These figures present cost and size trade-offs versus performance for the full range of specification requirements relative to random drift. Random drift was selected as the trade parameter because it is the dominant error source in most tactical missile applications where pre-launch alignment to a master inertial system is generally used.

1.3 RECOMMENDATIONS

The subject analysis coupled with on-going technology developments has evolved the following recommendations:

Performance Range	Sperry Model Laser Gyro
Low	SLIC-7 (Simplified)
Moderate	SLIC-7
Intermediate	SLIC-15
High	SLIC-15 or larger size model operating in the visible wavelength

Table 1-2. Performance/Cost Range Results

Parameter	Hi-Performance SLIC-22	Baseline SLIC-7	Lo-Performance SLIC-7 (triad)
Size-cubic inches/axis	234	47	47
Weight-pounds/axis	14	3.2	3.0
Cost-1978 dollars/axis	4,667	4,238	3,500
Performance:			
Bias uncertainty °/HR	0.02	0.5	3.0
Random drift $°/\sqrt{HR}$	0.005	0.05	0.1
Scale factor error PPM	5	100	250

As can be seen from the above, Sperry is recommending a change to the generic design to address the high performance requirements. The change is not dramatic from a physical configuration stand point. Instead of operating the gyro at the infrared transition, the visible transition is used. (All other features such as modular design, magneto-optic bias, etc remain the same.)

Theoretical analyses have been made that indicate that performance for a given size gyro will be improved by an order of magnitude with this wavelength change. Sperry currently has a 21 inch gyro operating at this wavelength with the magneto-optic bias and shortly will validate the improvement factor.

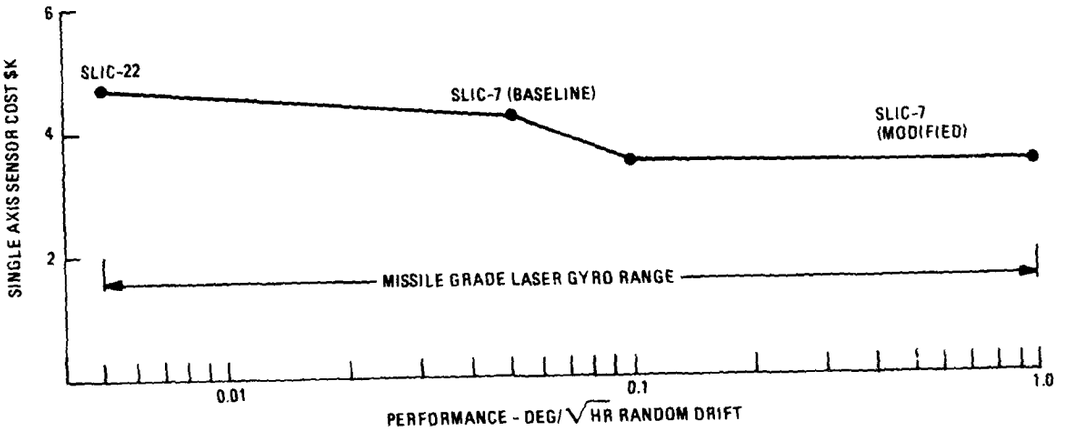

Figure 1-2. Cost Vs Performance

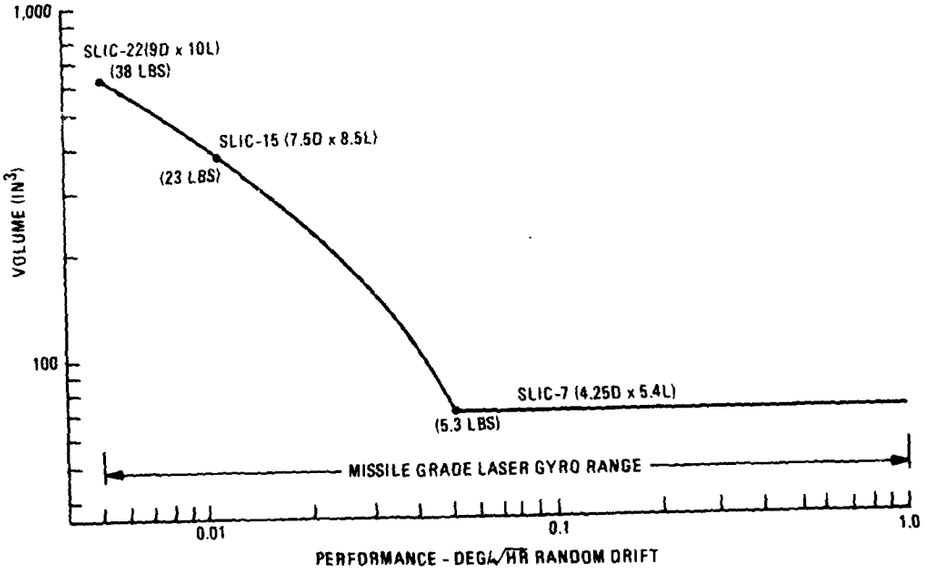

Figure 1-3. Size Vs Performance

Section 2

BASELINE LASER GYRO DESCRIPTION

2.1 BASELINE GYRO PHYSICAL DESCRIPTION

2.1.1 General Description

The baseline gyro consists of a SLIC-7 three-axis sensor assembly and a separate electronics assembly. The SLIC-7 three-axis sensor assembly contains three interweaved 7.5-inch resonant optical cavities that, when appropriately energized, measure input angular rotation. The electronics assembly provides the gyro excitation control functions and includes all the needed power conversions.

The sensor assembly, shown in figure 2-1, is cylindrical in shape and houses the optical assemblies of three gyros in a volume just over 70 cubic inches. The interwoven optical configuration employed establishes stable, mutual orthogonality between the gyros of the triad.

The electronics assembly, shown in figure 2-2, contains hybrid microcircuits, grouped functionally on circuit boards, and modular power supplies. It operates from +28 volts dc and delivers T^2L compatible pulse outputs from the three gyros. It also provides a single go-no-go discrete from internal BITE circuitry to indicate gyro operability status.

The electronics assembly configuration consists of a power supply and three gyro electronics cards that provide the control functions necessary for proper laser gyro operation.

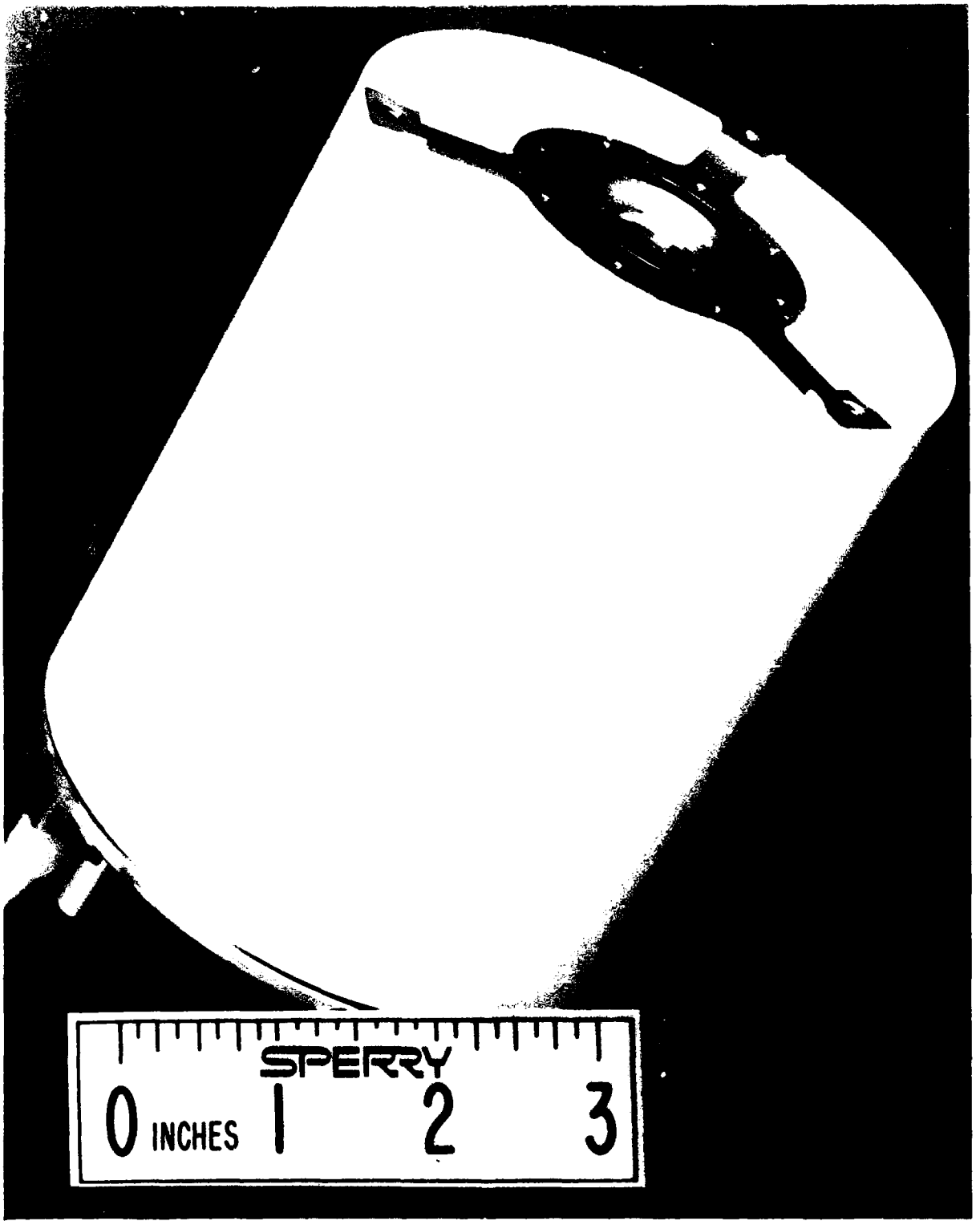

Figure 2-1 Baseline Gyro Sensor Assembly

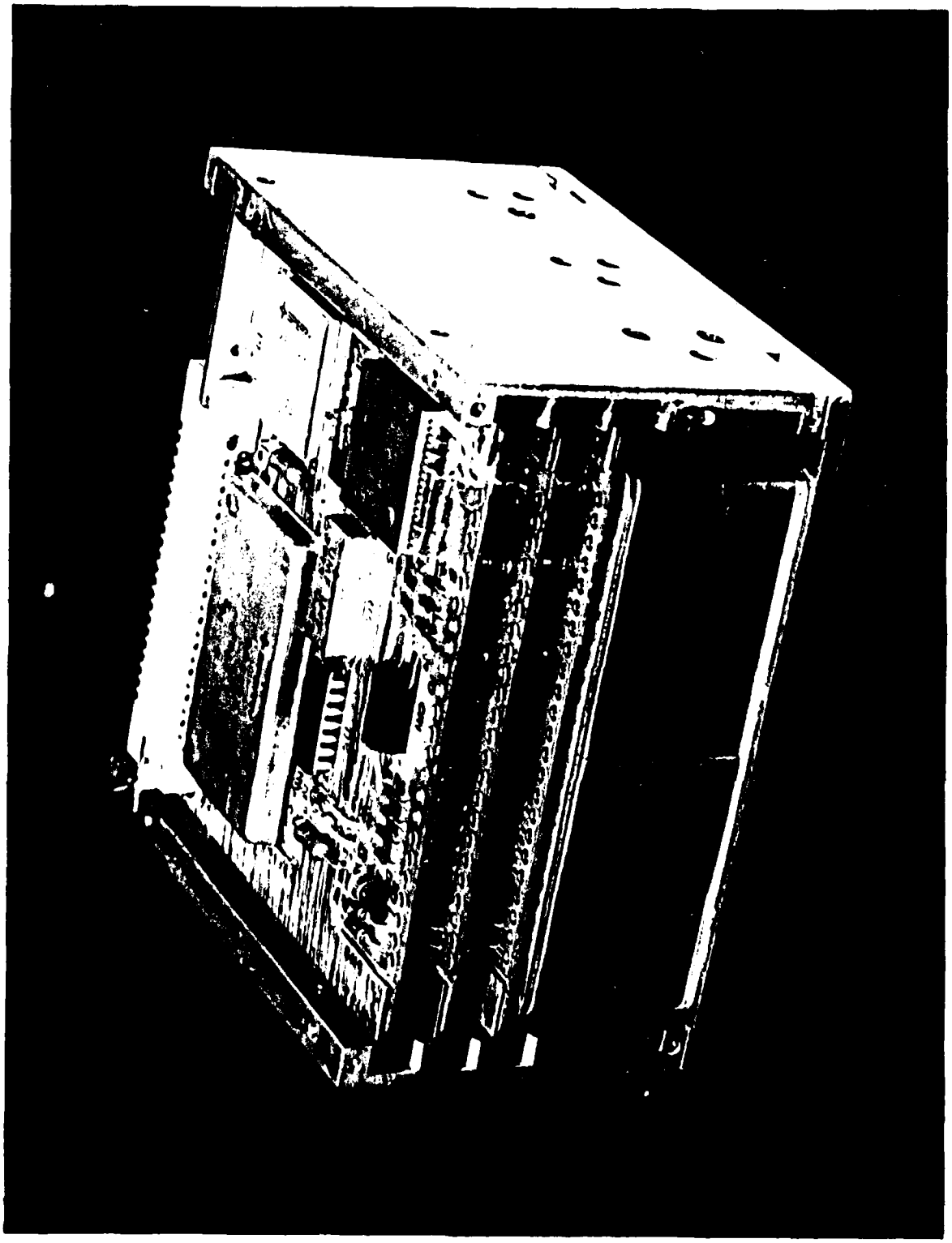

Figure 2-2. Baseline Gyro Electronics Assembly

Each gyro electronics card provides:

- Cavity path length control
- Optical bias regulation
- Discharge tube current regulation
- Precision voltage reference unit

Table 2-1 summarizes the baseline gyro physical characteristics. To arrive at the per-axis values noted, the three-axis values were divided by three.

To circumvent lock-in, the baseline gyro uses bias applied optically by the Sperry magnetic mirror. With this approach the gyro output frequency is proportional to the sum of the applied bias and the angular rotation rate about the gyro input axis.

This sine wave is converted into pulses, one for each positive and negative voltage swing (two pulses per cycle), and conditioned (T^2L buffers) for transmittal to a digital microprocessor for attitude computation. This incremental angle data (3.3 arc-sec/pulse) and measured sensor temperature data for compensations are used to compute vehicle body rates.

Figure 2-3 is a functional block diagram that shows the baseline gyro interface with a digital microprocessor. As shown the gyro incremental angles, analog temperatures and built-in-test discretes are outputted to the microprocessor for signal conversion into an accurate body rate measurement and a gyro operational status indication. In return, the microprocessor provides optical bias control discretes that establish the polarity of the magnetic mirror derived optical bias.

Table 2-1. Baseline Gyro Physical Characteristics

	Sensor Assembly (3 axis)	Electronics Assembly (3 axis)	Per Single Axis
Size (inches)	4.25 dia x 5.4 long	2.83H x 5.00W x 4.64L	-
Volume (cu. in)	75.2	65	46.7
Weight (lbs.)	5.3	4.3	3.2

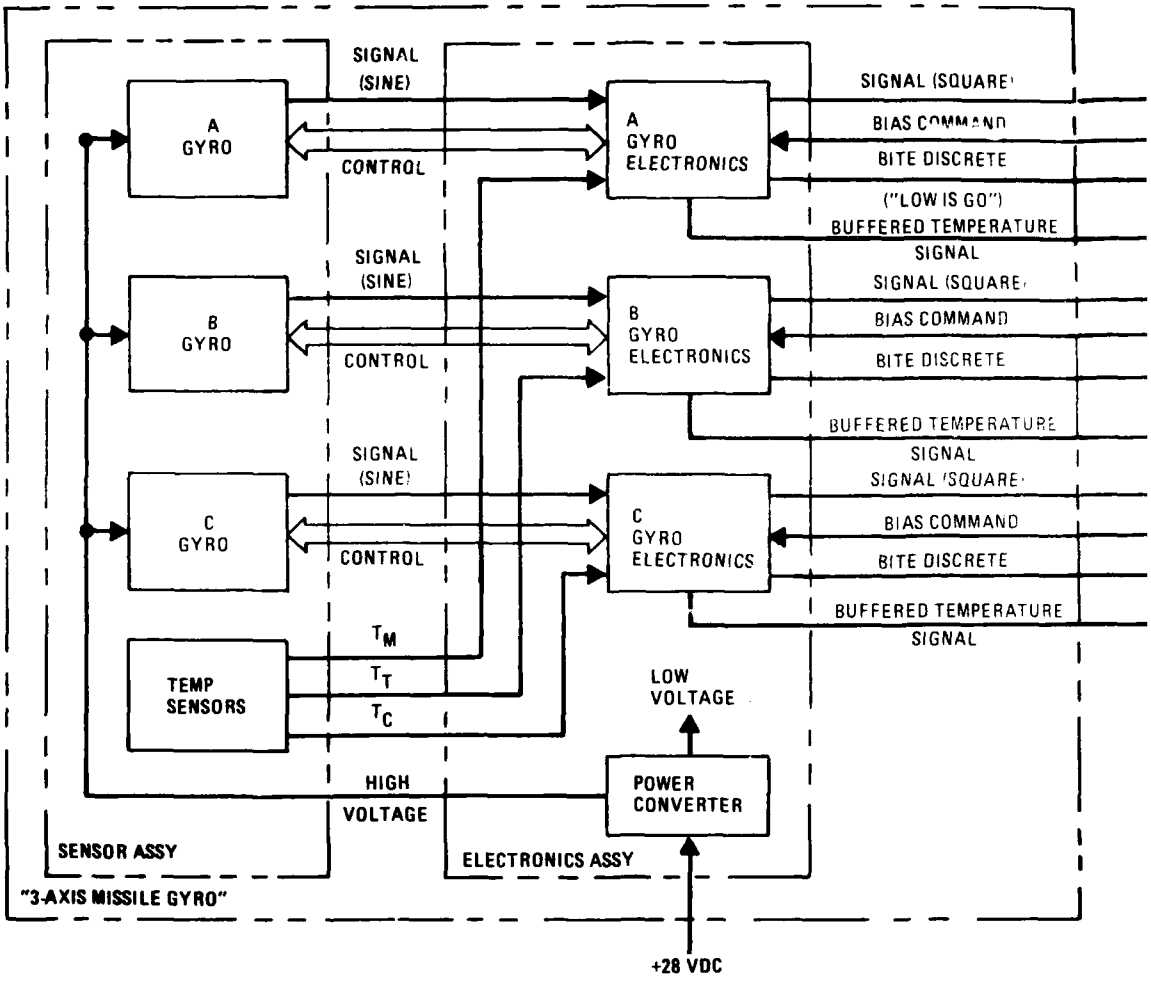
SIGNAL (SINE)
A GYRO
CONTROL
A GYRO ELECTRONICS
SIGNAL (SQUARE)
BIAS COMMAND
BITE DISCRETE
("LOW IS GO")
BUFFERED TEMPERATURE SIGNAL
SIGNAL (SINE)
B GYRO
CONTROL
B GYRO ELECTRONICS
SIGNAL (SQUARE)
BIAS COMMAND
BITE DISCRETE
BUFFERED TEMPERATURE SIGNAL
SIGNAL (SINE)
C GYRO
CONTROL
C GYRO ELECTRONICS
SIGNAL (SQUARE)
BIAS COMMAND
BITE DISCRETE
BUFFERED TEMPERATURE SIGNAL
TEMP SENSORS
T_M
T_T
T_C
LOW VOLTAGE
HIGH VOLTAGE
POWER CONVERTER
SENSOR ASSY
ELECTRONICS ASSY
"3-AXIS MISSILE GYRO"
+28 VDC

T_M
T_T
T_C

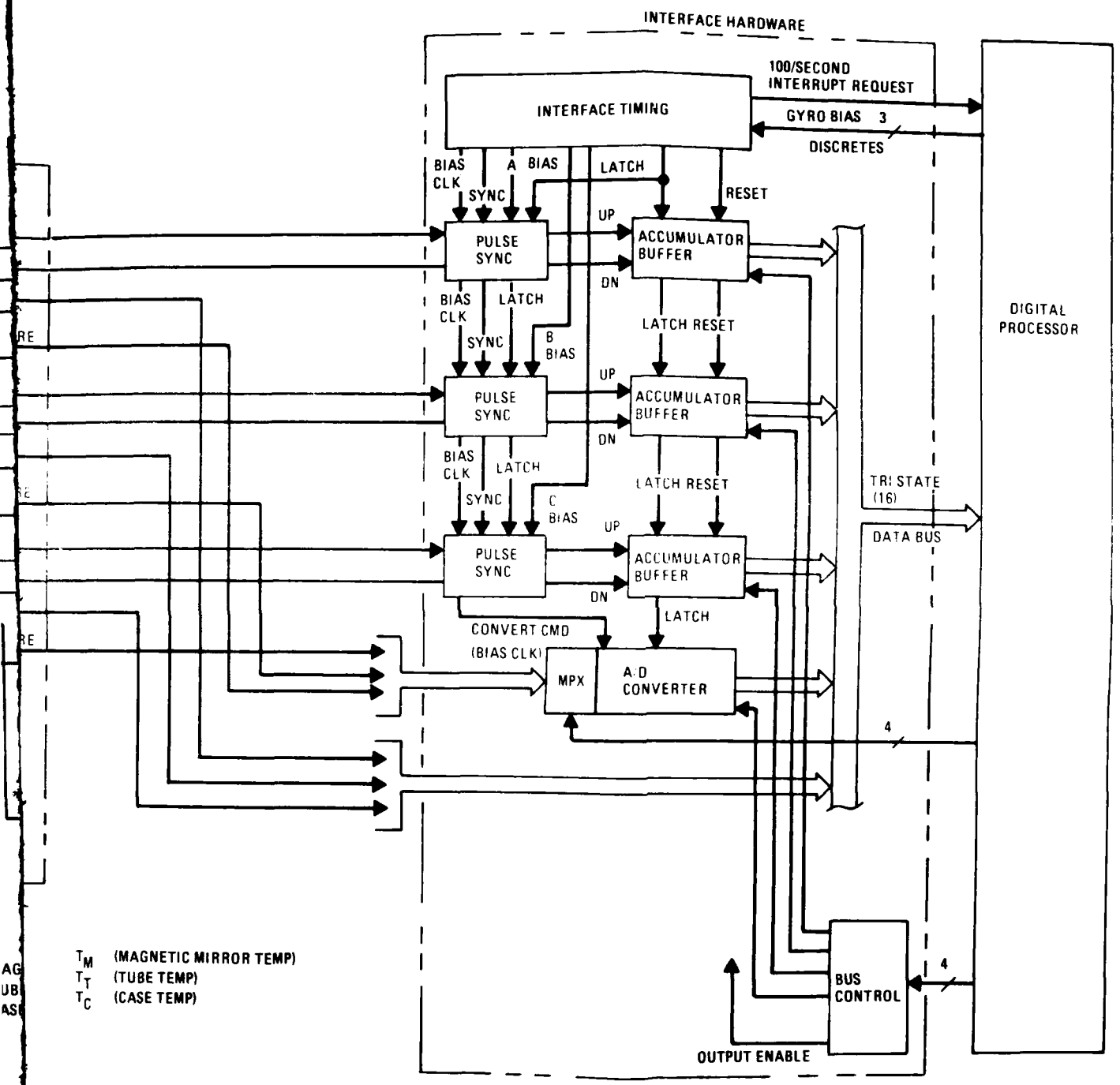

Figure 2-3. Functional Block Diagram
Missile IMU

2.1.2 SLIC-7 Sensor Assembly Description

The sensor assembly contains three laser gyros in a unique integrated design wherein the three laser gyros are machined into a single block of low expansion ceramic vitreous material so that their optical paths are interwoven. The basic gyro features a modular design approach in which the gyro elements (mirrors and discharge tube) are separable assemblies. This approach has been adopted because of the lower costs associated with increased production yield and service repairability.

The gyro triad consists of three identical 7.5 inch perimeter units mounted on a common block, such that the three sensitive axes are mutually orthogonal. This structural approach significantly reduces laser gyro size and makes a more rugged assembly. The laser gyro triad's volume is reduced to less than half of what it would be if single-axis gyros, of comparable performance, were used.

Additional advantages realized from the design are:

- Reduced cost - Many single axis assembly parts are eliminated and assembly operations performed once suffice for three gyros.
- Sensitive axis alignment and stability - A single rigid structure, precisely machined, orients the sensitive axes and guarantees alignment stability, an important strapdown consideration.
- Efficient inertial sensor packaging - A single enclosure efficiently houses three gyros.

Figure 2-4 is a photograph of the sensor assembly with cover removed. The basic dimensions of the unit, 4.25 inches in diameter by 5.4 inches long, translate into a weight of 5.3 pounds.

The integrated laser gyro triad structure, low expansion Owens Illinois CER-VIT, having a linear expansion coefficient of less than $\pm 0.3 \times 10^{-7}/^{\circ}C$, is constrained within its case by a single through-bolt, minimizing structural bending induced by thermal gradients. Two additional pins prohibit the triad from rotating with respect to its mounting surface. The components of the laser gyro are mounted directly on the optical structure.

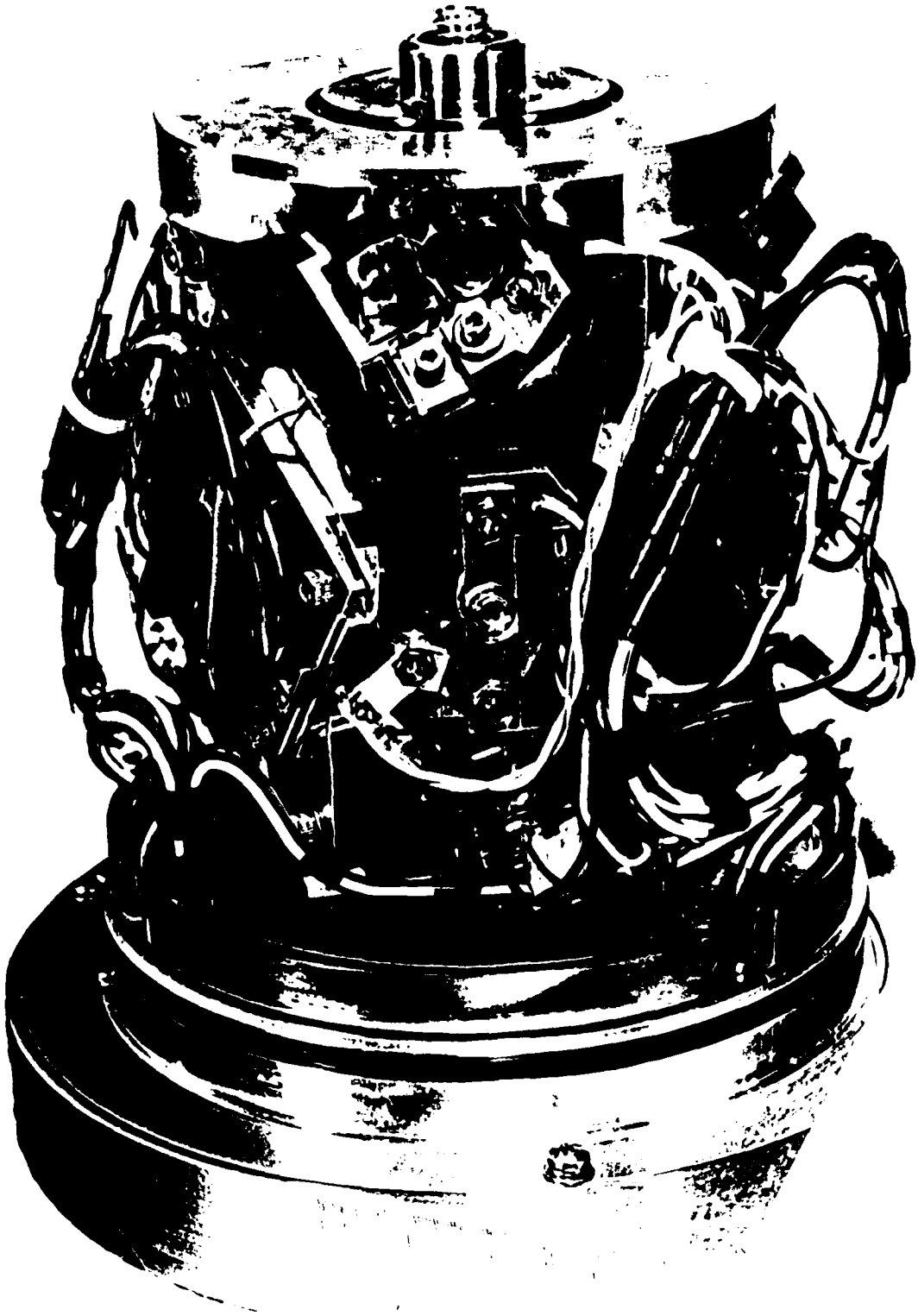

Figure 2-4. Baseline Gyro Sensor Assembly - Cover Removed

The three laser gyro optical cavities are machined out of a cylinder such that their input axes are orthogonal. The optical cavity of each gyro is approximately an equilateral triangle with a mirror mounted on each corner. Through-holes are bored into the block to form these triangles such that one leg of each gyro is inside one of the other gyros. This nesting of the gyro optical paths provides the compact size of this sensor assembly.

Note that one leg of each triangle is notched out to facilitate mounting the separable helium-neon discharge tube.

A two layer high-permeability shield surrounds the triad. This entire assembly is enclosed in a hermetically sealed aluminum case. (Laser gyros operate in a partial vacuum to minimize the influence of gas flow on gyro drift.)

The three laser gyros are identical. Figure 2-5 is an optical schematic diagram of the laser gyro. The input axis is normal to the plane of the page. The gyro consists of a closed, triangular optical path defined by three mirrors. Mounted in one leg of the triangle is a ceramic plasma tube filled with a low pressure mixture of helium neon gas. At each end of the tube is a glass window to permit light to pass through the tube (and therefore through the gas mixture). The gas mixture is excited by passing an electrical current through it, which excites neon atoms and results in the establishment of a clockwise and counterclockwise optical beam going around the optical cavity. The neon frequency employed has a wavelength of 1.15 microns (infrared).

When the optical cavity is not rotating, the clockwise and counterclockwise waves have the same frequency. But when the cavity is rotated, one path length is increased and the other decreased. The conditions for lasing require that total path around the cavity be an integral number of wavelengths and, therefore, the particular wavelength selected by the cavity for the clockwise beam is slightly different from the wavelength selected for the counterclockwise beam (one increasing and the other decreasing from the non-rotating value). The constancy of the velocity of light requires that the optical frequencies change also; the resulting difference between the clockwise and counterclockwise optical frequencies can be shown to be proportional to input angular rate. The count resulting from summing this frequency is proportional to the total angle through which the gyro has been rotated. The relationship between input

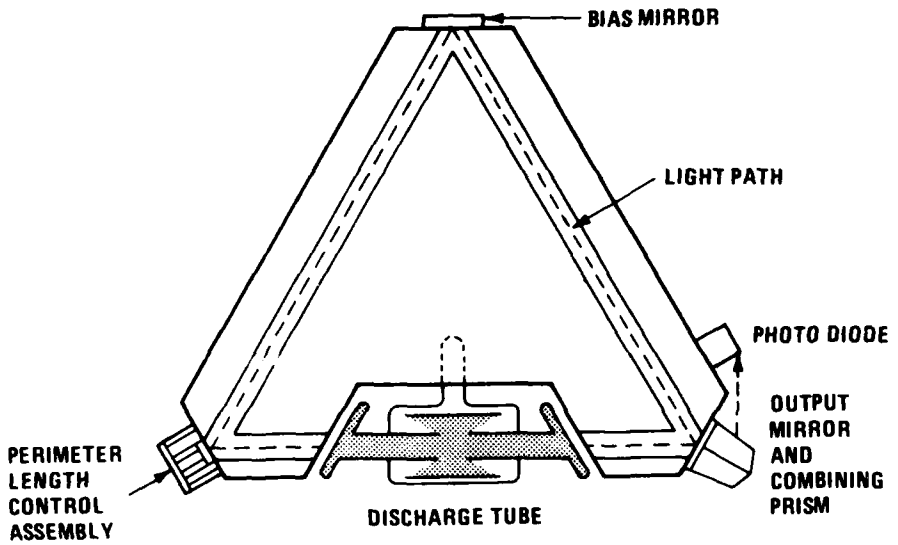

Figure 2-5. Baseline Laser Gyro (Generic) - Optical Schematic Diagram

angle and output count depends upon the size and shape of the optical path and the wavelength of the optical beam. In this case approximately 6.6 arc seconds of input angle result in an output cycle. (3.3 arc seconds per half cycle).

The mirrors defining the optical cavity have additional functions which are described below in detail.

The output mirror extracts optical information from the gyro. Its optical coating is specially designed to transmit approximately 0.1 percent of the incident light of both the clockwise and the counterclockwise beams. This is illustrated in the optical schematic diagram. The beams are totally reflected internally by the combining prism assembly and are superimposed on an optical coating (beam splitter) which is located on one of the prisms at the interface between the prisms. This coating reflects half of the incident light, and results in a combined beam which consists of a mixture of the clockwise and counterclockwise beams. The combined beam is intercepted by an optical detector that is alternately exposed to the sum of

CW and CCW optical amplitudes when the beams are in phase and is exposed to approximately zero input when the beams are out of phase. As the beams alternately come into phase at their optical difference frequency, the detector generates an electrical signal having a frequency proportional to input rate. The signal is amplified by a hybrid preamplifier mounted in the gyro case. (Each axis has its own separate preamplifier.)

The perimeter control mirror is used to servo the cavity perimeter to make it an integral number of the particular wavelengths for which the neon lasing medium has maximum gain. This insures maximum output and eliminates a medium-dependent source of error. The perimeter control mirror is mounted on a piezoelectric actuator consisting of two concentric cylinders mounted in push-pull fashion. Voltage across the cylinder thickness alters cylinder length and positions the attached mirror to effect the proper perimeter control. Perimeter control is achieved by oscillating the piezoelectric actuator mirror a small fraction of a wavelength (by exciting the actuator cylinders with alternating voltage) and, then, by applying a direct voltage to the actuator to eliminate variations in signal level at that alternating frequency. This insures operation at the peak of the gain of the lasing medium.

The third mirror, the bias mirror, introduces an apparent rotation in the gyro to bias the clockwise and counterclockwise frequencies away from each other. This avoids the non-linear (around zero input rate) laser gyro operating region caused by energy coupling between the two counterrotating light beams. Without biasing, the coupling makes the light beams lock to the same optical frequency and results in a laser gyro rate threshold. A magnetic crystal coating the mirror, when saturated by an applied magnetic field, causes a differential clockwise-to-counterclockwise phase delay and biases the gyro CW and CCW optical frequencies away from locking. This bias is extracted from gyro information prior to its use. To eliminate the effect of long term drift of the applied bias, the sense of bias is periodically reversed by reversing the coil excitation that generates the magnetic field.

The source of gyro gain is the plasma tube. The plasma tube is a ceramic structure sealed by using brazed ceramic-to-metal joints and containing a low-pressure mixture of helium and neon gases. The gas mixture is excited by passing an electrical discharge through it from two anodes to an aluminum cold cathode. At each end of the tube is a metal anode assembly containing an optical window.

2.1.3 Electronics Assembly Description

The function of the baseline gyro electronics, shown in figure 2-2, is to provide the closed loop control necessary for proper laser gyro operation. In addition, it converts the primary 28 volts dc supply into the appropriate operating voltages.

The gyro control electronics provide optical bias current, discharge tube current, and cavity path length control for each laser gyro axis. These functions are channelized so that a single electronics card is provided for each axis. Figure 2-6 is a photograph of the gyro control card (three used per baseline sensor). A detailed description of the gyro control electronics is contained in subsection 2.1.3.1.

The power supply used in the electronics assembly is a multiple output dc-to-dc converter which converts the 28 volts dc input to the regulated dc voltages required for proper three-axis rate sensor operation. The power supply and power requirements are discussed in subsection 2.1.3.2.

The three gyro circuit boards and the power supply are packaged in a rectangular box 4.64 inches long by 5.00 inches wide by 2.83 inches high which weighs 4.3 pounds.

2.1.3.1 Gyro Control Electronics

The laser gyro control electronics are designed to provide the following three closed loop functions:

- Discharge current regulation
- Cavity path length control
- Optical bias control

Discharge Current Regulation

Each ring laser optical cavity contains a cold-cathode double anode He-Ne gas discharge tube to provide lasing energy. This tube requires approximately -2000 volts to cause tube ignition for operation. When the tube fires, the excitation voltage is on the order of -1000 volts to sustain operation. The function of the discharge current regulator circuit is to provide the starting (breakdown) voltage and then control the magnitude of the discharge tube current to a preset value during sustained operation.

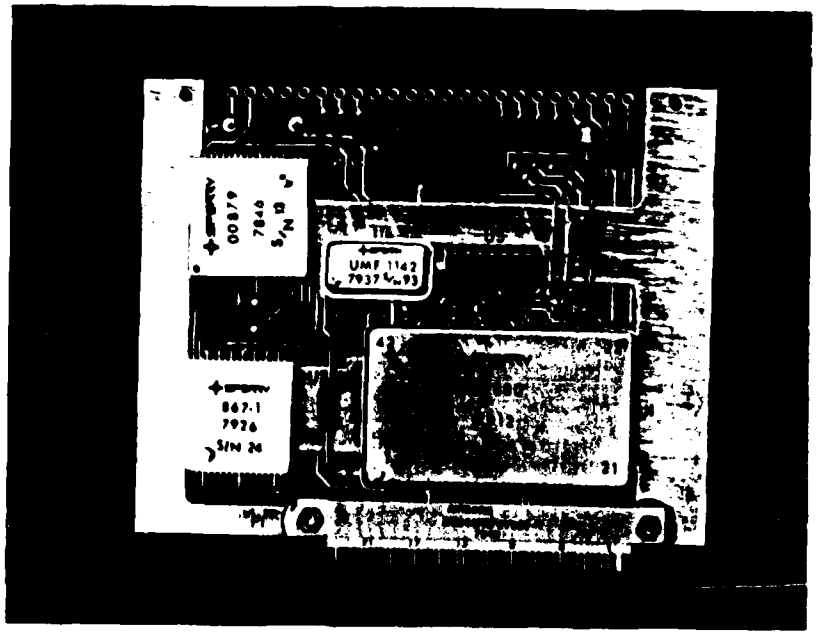

Figure 2-6. Gyro Control Electronics Card

In addition to controlling the magnitude of the total (cathode) current, the regulator also controls the ratio of anode currents in the laser tube. The anode currents are individually sensed and controlled. One controller senses the difference of the anode currents and maintains it at a constant level. Another controller compares the sum of the anode currents to a stable precision voltage reference and adjusts the total (cathode) current flow to a fixed constant. A block diagram of the discharge current regulator is shown in figure 2-7. The unit is contained in a 1 inch x 1 inch hybrid flat pack.

Cavity Path Length Control

The cavity path length control stabilizes the oscillation frequency of each laser at the maximum gain of the lasing medium. In a normal configuration, the ring laser gain curve, as a function of cavity perimeter, has a shape similar to the 0 to 180 degree portion of a sine wave. The desired operating point is at the 90 degree point, which corresponds to a specific cavity perimeter. The controller operates on an error signal obtained by changing the cavity perimeter using an ac-excited piezoelectric actuator upon which a corner reflector is mounted.

Assuming the cavity is exact, the application of the piezoelectric actuator motion will provide no output signal for the servo channel from the ring preamplifier. This result is obtained because the motion amplitude is less than 0.1 wavelength and the actuator excursions occur over the relatively flat portion of the sine wave peak. If the cavity is not at the precise center of the gain curve, the motion causes an error signal output from the ring preamplifier. A phase detection of this error provides a signal proportional to the magnitude and direction of lasing frequency from maximum gain center. The error signal is amplified and summed with the ac reference voltage to produce a dc component to adjust the position of the piezoelectric actuator toward gain center. The loop gain determines the accuracy with which this correction can be made.

In the steady state condition, any disturbance that causes the perimeter to be other than at gain center will require a finite error signal to provide the perimeter compensation. To eliminate this steady state error, a pseudo integrator is used to build up an output signal approximately equal to the error signal, thereby driving the error signal towards zero. A block diagram of the cavity path length control is shown in figure 2-8. The unit is contained in a 1.4 inch x 2.3 inch hybrid DIP pack.

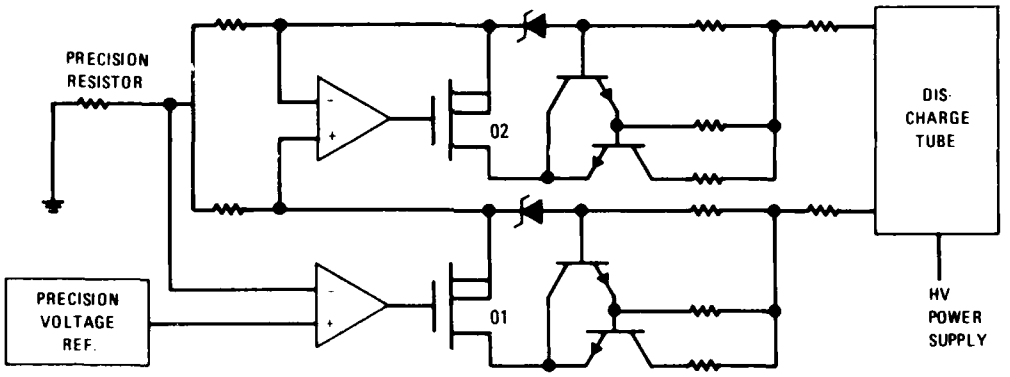

Figure 2-7. Discharge Current Regulator

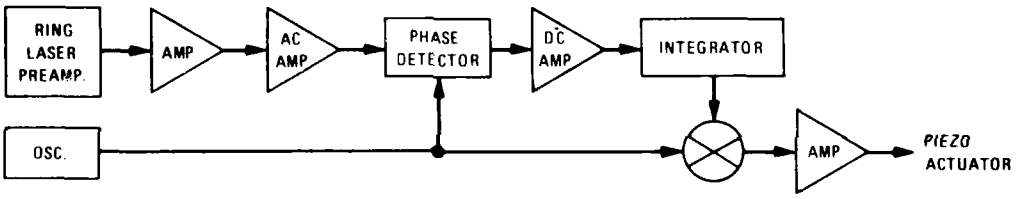

Figure 2-8. Path Length Control

Optical Bias Control

The function of the optical bias control electronics is to apply a precise reversible dc current to the laser gyro bias cell coil in response to an external discrete. Precise current control, from both a repeatability and stability basis, is provided over the specified temperature range. The requirements on stabilization of the absolute value of the applied bias can be reduced by periodically reversing the direction of the applied bias because any long term shifts in the bias characteristics cancel. In actual operation, bias current reversal occurs at approximately one-second intervals. The switching speed is, therefore, important to allow current stabilization at the dc level for essentially the whole interval. A block diagram of the optical bias control is shown in figure 2-9. The unit is contained in a 1 inch x 1 inch hybrid flat pack.

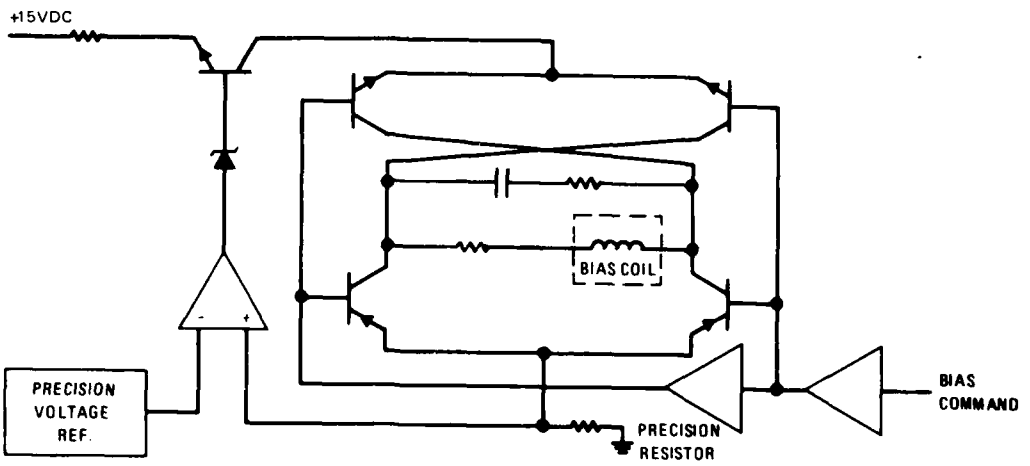

Figure 2-9. Optical Bias Regulator

The precision required by the regulating circuitry is provided by the reference hybrid. This unit contains precision operational amplifiers and low temperature coefficient resistors which supply excitation to an external precision reference diode. The reference diode is located in a component temperature stabilizer.

2.1.3.2 Power Supplies

The baseline laser gyro power supply is designed to convert unregulated 28 volts dc into the regulated dc voltages required for proper three-axis rate sensor operation. This is accomplished by using a custom designed multiple output dc to dc converter that contains EMI/RFI filtering and over voltage and short circuit protection.

The high voltage required for the laser discharge tubes is obtained from an output that delivers -2000 volts for tube ignition. Once the tube is ignited, the tube power supply output is clamped to -1000 volts for sustained operation. This two-step voltage arrangement minimizes power dissipated for discharge current regulation. During operation, each tube requires between 0.5 and 1.0 mA of discharge current,

which is supplied by the clamped -1000-volt output. This discharge current is precision regulated as previously described in the laser gyro control electronics discussion.

The +240 volts dc is used by the amplifiers which drive the piezoelectric actuators in the path length control servo.

The low voltage power required by the electronics unit is provided by ±15 volt outputs which supply the excitation for various operational amplifiers and linear circuitry.

The power supply is mounted on the rear plate of the electronics unit where the frame provides the necessary heat conduction.

The baseline missile gyro power dissipation is summarized in table 2-2.

2.2 BASELINE GYRO PERFORMANCE

The performance of the baseline gyro over the required environmental range is to be established by the extensive testing planned by the Naval Weapons Center. Test data taken on the baseline gyros at Sperry confirm that the performance of the SLIC-7 baseline gyro is better than the program's performance objectives as shown below.

	Baseline Gyro Performance (1σ)	
Supply Function	Objective	Measured
Bias uncertainty °/HR	1.0	0.35
Random drift °/$\sqrt{\text{HR}}$	0.13	0.05
Scale factor error PPM	250	64

The test data that shows the baseline performance is presented in section 3.3.1.

Table 2-2. Three Axis Power Requirements

	Volts, DC	Power, Watts
Discharge tube ignition	-2000	0.3
Discharge tube sustained	-1000	3.0
Piezoelectric actuator excitation	+240	2.4
Operation amplifier excitation	±15	7.2
Total Output Power		12.9
28 Volt Input Power (50% Avg. Eff.)		25.8

2.3 BASELINE GYRO PRODUCTION COST ESTIMATE

The laser gyro provides the base for the development of an extremely low cost inertial system. Its characteristics make it an ideal strapdown sensor that eliminates complex mechanical parts with their inherent unreliability. Its inherent digital output, minimizing computer interface equipment, reduces the system to two elements: sensors and computer. This digital strapdown system has the flexibility to readily accommodate the fast-paced improvements in both the computer and sensor area. The computer technology is advancing rapidly towards smaller, faster and lower cost machines. The result will be modular, micro-programmable mini-computers that can easily accommodate the strapdown computations with the other guidance requirements.

The baseline laser gyro is cost effective because of its relative simplicity in terms of total number of parts with a minimum that are precision machined. This translates into a minimum of skilled "touch" labor, which buffers the cost against rising labor rates.

An additional cost advantage is the modular construction utilized in the baseline design. The modular components are mass produced and tested prior to optical assembly, assuring a maximum production yield.

A unit production cost estimate, for a quantity of 700 units (2100 axes) produced at 30 per month, was generated for the baseline laser gyro. The results of this estimate are summarized in table 2-3 with a detailed breakdown presented in Appendix A.

The baseline gyro consists of two separate assemblies: a sensor assembly and an electronics assembly. The sensor assembly is the Sperry SLIC-7 three-axis configuration part number 6077074. The electronics assembly, part number 6077072, contains hybrid circuits and a power supply. Estimates to produce these equipments were made using 1978 dollars in accordance with the statement of work. As shown in the table, the SLIC-7 cost is $12,715 for the three axis configuration, which, when divided by 3, gives the per axis cost of $4,238.

Figure 2-10 has been prepared to show the separation of labor and material costs on a percentage breakdown. The baseline gyro costs are 61% material and 39% labor, which reflects the small amount of touch labor associated with laser gyro manufacture.

Table 2-3. Baseline Gyro Cost estimate (1978 Dollars, 16% G&A, 10% FEE)
(Three Axis Assembly)

	Sensor Assy P/N 6077074	Electronic Assy P/N 6077072
Material	3691.47	4059.67
Machining	572.92	118.78
Assembly	1068.01	442.19
Inspection & Test	819.19	206.99
Engineering & QC	1379.36	356.34
	$ 7530.95	$5183.97

TOTAL UNIT COST $ 12,714.92

PER AXIS COST 4,238.31 (1978 Dollars)

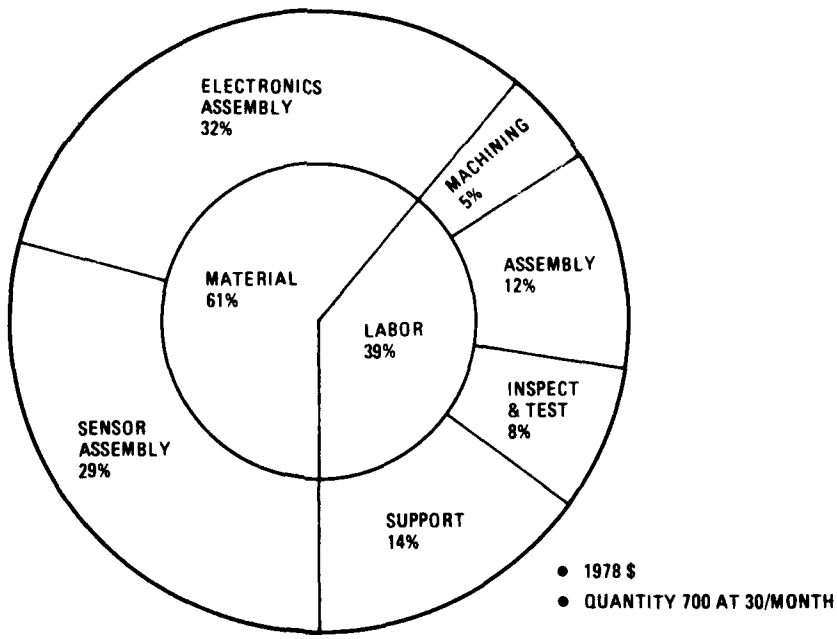

Figure 2-10. Baseline Cost Estimate

Design approaches to laser gyro lock-in circumvention differ between manufacturers. The Sperry approach, described in detail in section 2.1, employs a magneto-optic bias element that is operated in two saturated output states: a plus and a negative output. The basic gyro output contains both the vehicle input angular rate plus that provided by the magneto-optic element.

This implementation imposes some software burden that is peculiar to this bias approach. Figure 2-11 is a functional block diagram showing the recommended software implementation to convert the laser gyro output to corrected body angular increments. Table 2-4 tabulates the computer burden, speed and memory requirements, for complete software correction.

As shown in figure 2-11, three of the functional blocks are common to all laser gyro configurations. The peculiar functions required by the switched DC magneto-optic approach are the bias cycling and bias tracking functions. As shown in table 2-4, these additional functions add an insignificant time burden (1%) and 202 memory words.

If it is assumed that all other configurations of laser gyros have only the common software functions noted (with these memory and time burdens), then the Sperry baseline gyro costs should be incremented to provide for the extra memory. At an estimated cost of 1 dollar per word the cost of each three-axis configuration should be increased by $202 or $67/single axis.

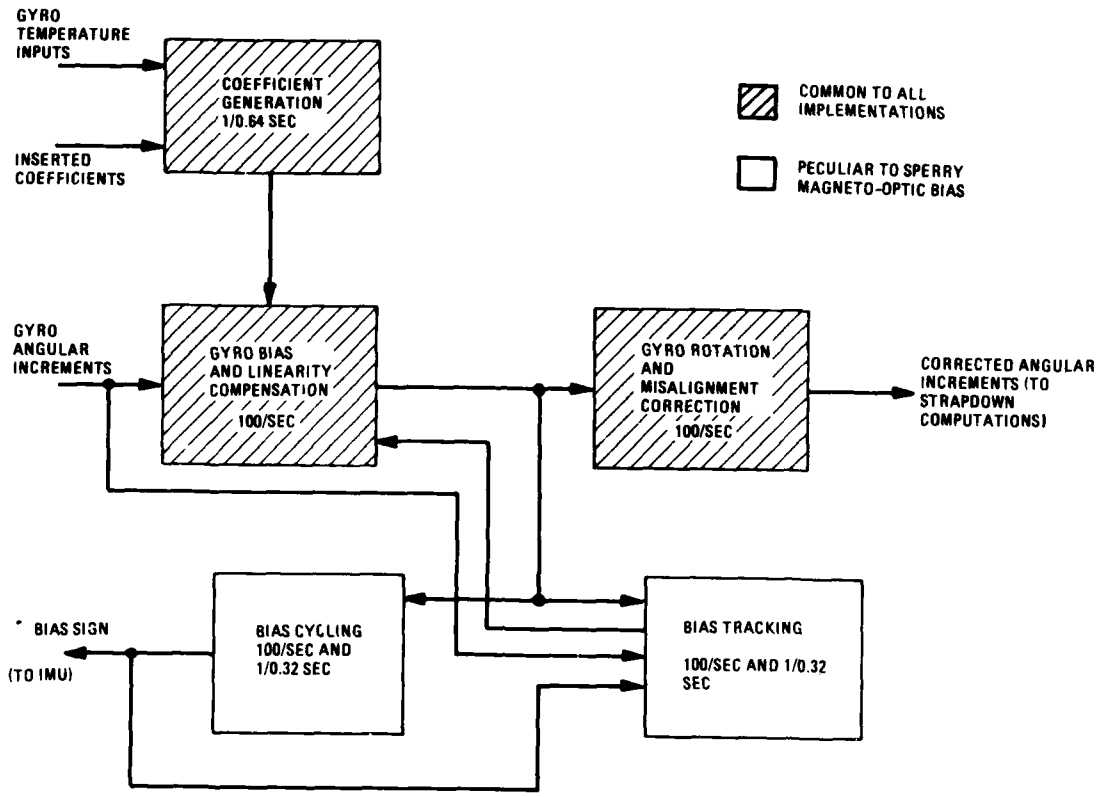

Figure 2-11. Front End Software Computational Flow Diagram

Table 2-4. "Front-End" Computing Burdens

		Operations per Second
Operations	Total	Bias Cycle & Bias Tracker
Adds	320	2
Multiplies	1860	18
Divides	300	0
Data processor adds	3370	356
Other orders	20170	8930
Timing burden (SP-2000 with firmware multiply)	0.047 sec/sec = 4.7% of time	0.0096 sec/sec = 1% of time
Memory words (16 BIT)	PROM=400	PROM=202

Section 3

BASELINE GYRO DESIGN PERFORMANCE/COST RANGE ANALYSIS

3.1 SUMMARY

The missile grade laser gyro specification specifies a performance range requirement that must be satisfied by the generic baseline gyro design.

To provide laser gyros that cover this performance spectrum, size is traded off. Laser gyro performance is a function of the area encompassed by the optical path. For the baseline SLIC-7 laser gyro the optical path is 7.5 inches for essentially an equilateral triangle. If the triangular geometry is retained, gyro performance becomes a function of its optical path length. The SLIC-7's one sigma performance capability is described by the following key parameters:

- Drift repeatability 0.5°/HR
- Random drift $0.05°/\sqrt{HR}$
- Scale factor 100 PPM

The following paragraphs contain the data used to define two derivatives of the baseline gyro. One configuration is presented to satisfy the highest performance requirement specified. The gyro would be identical to the baseline except its optical perimeter is increased by approximately a factor of 3. The interweaving configuration would be retained and this three-axis gyro would be called a SLIC-22.

For the lower performance application a gyro smaller than the SLIC-7 was not considered due to practical considerations relative to the modular arrangement where there is a finite limitation on discharge tube size reduction. What is proposed for the lower range is a ' stripped down" version of the baseline gyro. Modifications are presented that reflect in reducing the cost.

The results of these analyses are presented in table 3-1. The interwoven three-axis design of the baseline gyro is used for all gyros. To provide a ready comparison to the specification requirements, the size and cost data are presented per axis (1/3 the total cluster).

The paragraphs that follow present the scaling laws used in determining the generic laser gyro performance dependence on its size. Data are included that validate these scaling laws based on test results obtained on three different perimeter size gyros: 7.5 inch (SLIC7), 15 inch (SLG15) and 21 inch (SLG21). These laws are then used to establish the high performance SLIC22 gyro. The basis for the estimated cost of the high and low performance gyros is then presented.

3.2 LASER GYRO SCALING LAWS

3.2.1 Error Mechanisms and Status Summary

The performance of a laser gyro is size dependent with most errors inversely proportional to the area enclosed by the lasing path. Since the control electronics and component parts cost are practically independent of linear dimension, it is usually effective from a cost versus performance consideration to maximize the enclosed area to the weight/volume limits imposed on the system. Sperry's interleaved gyro cluster permits the largest possible gyro size/system size ratio and, thereby, maximizes performance versus volume for inertial systems requiring at least three axes of sensed rotation.

Table 3-1. Performance/Cost Range Laser Gyros
(Per Axis Characteristics)

Parameter	SLIC-22	SLIC-7 (Baseline)	SLIC-7 (Trimmed)
Size (cubic inches)	234	47	47
Weight (pounds)	14	3.2	3.0
Cost ('78 dollars)	4667	4238	3500
Performance:			
Bias uncertainty (°/HR)	0.02	0.5	3.0
Random Drift (°/$\sqrt{\text{HR}}$)	0.005	0.05	0.1
Scale factor (PPM)	5	100	250

Table 3-2 lists most of the error sources of the laser gyro, including their control techniques, and the relative importance of the residual errors after application of the control techniques. Errors are classified as bias drift, scale factor, and random (or white noise) drift. Errors due to stationary processes can be calibrated out, and the primary determinants to system performance are the turn-on-to-turn-on repeatability of the residual errors, as well as long term stability of calibration. Except for random drift, all laser gyro errors are causal - i. e. the results of dimensional, thermal, or electrical inputs, and could, in principle, be compensated if the gyro could be accurately modeled. The present thrust of gyro improvement is to reduce the sensitivity of the gyro to disturbing inputs (for example, by reducing cavity loss) and to shield the gyro from such disturbing inputs (such as stray magnetic fields and thermal gradients). Only a limited amount of dynamic modeling is used for error correction (i. e., temperature measurements of the tube and magnetic mirror).

The subsections which follow discuss the error models for the non-negligible error mechanisms and how they scale with perimeter length.

At this point in time, Sperry has tested three different size laser gyros of the same basic design with similar garnet bias mirrors, all at 1.15 micron: the SLIC-7 (nominal 7.5 inch perimeter), the SLG-15 (nominal 15 inch perimeter), and an SLG-21 (nominal 21 inch perimeter). Only the SLIC-7 has been tested over a wide environmental range. Therefore, for scaling law comparisons, performance measured in the same type of laboratory room environment was utilized. Residual errors due to imperfect compensation of temperature effects will add somewhat to the performance discussed herein. Table 3-3 presents a summary of the performance being exhibited at this time by the gyros that have been tested. The supporting data are given in later subsections of this report. Various design improvement investigations are underway to improve on this performance, such as the use of apertures (to enable higher cavity power without excessive off-axis modes), operation in the visible (0.633 micron) domain (for the larger perimeter units), the use of quartz tube windows, and many more. However, none of these improvements are considered here since they are not incorporated in the baseline SLIC-7 unit.

Table 3-2. Potential Error Mechanisms

Gyro Performance Error	Potential Error Producing Mechanism	Error Control Techniques	Residual Error
Bias Drift	Optical path length shift from gain center	• Closed loop servo control of optical path length	Negligible
	Fresnel drag effects in optical cavity	• Evacuate cavity	Negligible
	Magnetic sensitivity	• Magnetic shielding	Small
	Active medium flow in discharge tube	• Split discharge • Discharge current regulation • Tube design and gas fill selection • Thermal conductive shielding • Temperature gradient compensation	Important
	Non-reciprocal backscatter coupling combined with non-reciprocal loss	• Ultra low scatter optics • Minimize non-reciprocal loss of bias element	Small
	Magnetic mirror reversal unbalance	• Optimize electromagnet design	Important
	Shift in backscatter coefficient turn-on to turn-on	• Dimensionally stable optical cavity • Ultra low scatter mirrors	Small
Random Drift	Phase fluctuations due to spontaneous emission	• Optimize design parameters • Low loss optical components	Important

Table 3-2. Potential Error Mechanisms (Cont)

Gyro Performance Error	Potential Error Producing Mechanism	Error Control Techniques	Residual Error
Scale Factor Error	Optical path length shift from gain center	• Closed loop servo control of optical path length	Negligible
	Optical backscatter coupling	• Ultra low scatter optics	Important
		• Optical bias well away from lock-in region	
		• Cavity dimensional stability	
	Cavity Q and lasing intensity	• Aging resistant mirrors	Important
		• Low loss optical components	
		• Long life tubes	
		• Discharge current regulation	

Table 3-3. Sperry Laser Gyro Performance Current Status Summary

All garnet bias mirror, 1.15 micron triangular cavities, laboratory room environment	White-Noise Random Drift deg/$\sqrt{hr}$ rms	Turn-On Drift Repeatability (deg/hr) (1σ)	Scale-Factor Error (PPM) (1σ)
Joint service missile grade RLG range requirement	0.005 to 1.0	0.02 to 3.0	20 to 500
SLIC-7	0.051	0.35	64
SLG-15	0.011	0.048	10
SLG-21	0.0056	Not measured	Not measured
Empirical scaling law with perimeter length	$\frac{1}{p^2}$ (See figure 3-1)	$\frac{1}{p^{2.8}}$	$\frac{1}{p^{2.7}} \mid k\frac{\Omega_t^2}{\Omega_m^2}$
Theoretical scaling law with perimeter length	$\frac{1}{p^2}$	$\frac{1}{p^2}$	$\mid k\frac{\Omega_t^2}{\Omega_m^2}$

A theoretical scaling law for scale-factor error with perimeter length has proven to be difficult to arrive at. It can be shown that the dominant scale-factor error in an optically biased ring is given by:

$$S.F.E = k\frac{\Omega_t^2}{\Omega_m^2}$$

where Ω_t = lock-in threshold rate

Ω_m = magnetic mirror bias rate

k = proportionality constant

In other words it is best to operate as far away from the lock-in zone as possible as far as scale factor error is concerned.

This relationship is listed in table 3-3 and it has been verified empirically.

3.2.2 Random Drift Rate Error

Laser gyros are characteristically noisier in performance than conventional wheel gyros. Drift noise can arise from many sources, including noise in the discharge current from plasma oscillations, poor regulation, poor path length perimeter control, beat note phase disturbance through bias reversal, output pulse conversion and counting errors, incomplete and erratic magnetization of the bias element, and spontaneous emission noise in the laser modes.

Careful design will eliminate most of the above errors, leaving only more fundamental sources such as spontaneous emission noise and lock-in effects.

The Sperry square wave bias approach does not allow noise to arise from lock-in effects, as the bias is reversed relatively seldom and with practically instantaneous speed. However, Sperry rings, as do all laser gyros, exhibit a white noise type of random drift, which is ascribed to laser spontaneous emission.

Starting with the premise that the zero-point energy of a cavity mode is $1/2\ h\nu$, the resulting amplified noise causes a phase wander of the beat signal given by:

$$(\Delta\psi)^2 = \frac{1}{2}\left[\frac{c}{p}\right]^2 h\nu\ \frac{\delta}{W}\ t \qquad (3.1)$$

where $\Delta\psi$ = probable phase error

$c = 3 \times 10^8$ meters/second

p = cavity perimeter, meters

h = Planck's constant

ν = lasing frequency, c/λ, Hz

δ = fractional power loss of cavity

W = in-cavity lasing power level, each wave, watts

t = total measurement time, seconds

Using the nominal ring laser scale factor equation

$$f = \frac{4A}{\lambda p}\Omega \qquad (3.2)$$

for a triangular ring, where Ω is rotation rate about the input axis and A is area enclosed by laser gyro path, the probable drift angle error in degrees is given by:

$$\theta = 2.7 \times 10^{-4} \frac{\lambda^{1/2}}{P^2} \left(\frac{\delta}{W}\right)^{1/2} T^{1/2} \qquad (3.3)$$

where θ = output angle error in degrees, rms

λ = wavelength in microns

T = measurement time, hours

P = cavity perimeter

or white noise random drift $A_N = K_N \frac{\lambda^{1/2}}{P^2} \left(\frac{\delta}{W}\right)^{1/2}$ deg/$\sqrt{Hr}$ (3.4)

This scaling law has been verified many times in Sperry's laser gyros. The major performance achievement attained by the recent substitution of the garnet magnetic bias mirror for the metallic coated type was the marked reduction in the cavity loss δ. This has led to a corresponding marked reduction in the white-noise random drift for a given magnetic mirror bias value.

A major limitation in white-noise random drift in Sperry infrared gyros is that cavity power, W, is increased (excess of discharge tube driving current over that needed to achieve lasing) to a maximum point above which intolerable off-axis modes are generated. Apertures (to attenuate the off-axis modes) are being investigated to enable larger cavity power operation.

Figure 3-1 is a pictorial representation of the white-noise scaling law, using 0.01 deg/$\sqrt{hr}$ for a 15-inch perimeter laser gyro at 1.15 micron wavelength as a base-point. Plotted on this scaling diagram are actual data points measured on 7.5-inch perimeter, 15-inch perimeter, and 21-inch perimeter units, all operating at 1.15 micron infrared and all employing garnet magnetic mirrors. Close agreement with the (perimeter length)^2 accuracy relation is observed.

3.2.3 Bias Drift Rate Errors

Bias drift repeatability is defined as the rms variation of average drift rate of the gyro from turn on to turn on. The average drift rate itself is compensated by the system as are various temperature related drift phenomena, employing coefficients obtained at the last calibration.

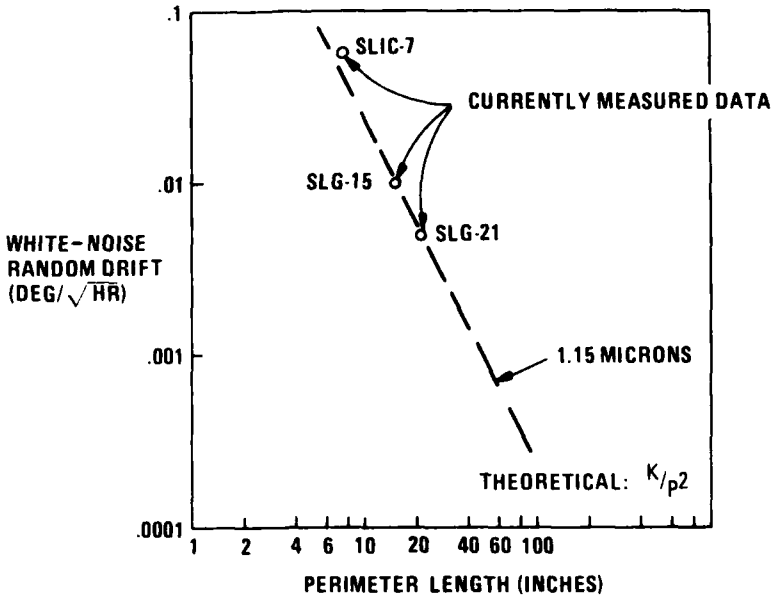

Figure 3-1. White Noise Random Drift Vs Perimeter Length

By far, the largest sources of drift in a laser gyro arise from the properties of the laser gyro gain medium. Apertures, intended or otherwise, optical backscatter changes in the presence of non-reciprocal cavity loss, and magnetic mirror reversal imbalance can also cause drift changes. These phenomena are described in the following subsection.

3.2.3.1 Active Medium Phenomena

The following paragraphs discuss drift mechanisms intrinsic to the active medium. Such mechanisms are the dominant source of gyro drift instability. The properties of the active medium which give rise to drift are the following:

- Magneto-activity (high Faraday rotation)
- Optical dispersion
- Active medium flow
  - DC discharge induced
  - Thermal gradient induced

The magneto-optic properties of the gas laser medium are related to the optical dispersion of the spectroscopic transition being used as the gain wavelength, and to the line splitting that results from application of axial magnetic field (the longitudinal Zeeman effect). A detailed discussion of active medium magneto activity is beyond the scope of this report. Suffice it to say that an active laser medium, when exposed to a weak magnetic field aligned with the direction of light propagation, exhibits a magnetic circular birefringence proportional to the gain of the medium multiplied by the strength of the magnetic field. Every attempt is made to maintain purely linear polarization in the active medium to minimize the sensitivity of drift to stray magnetic fields. In addition, magnetic shields are used to attenuate stray fields.

Axial flow of the active medium is a potentially large source of drift error in a laser gyro. The active medium has a gain which is wavelength dependent. A frequency sensitive gain implies an index of refraction which is frequency sensitive. The dependence of index on frequency is linear near gain center frequency with positive slope.

Flow of the active medium in a laser gyro has the following effect. The wave traveling with the medium is doppler down-shifted in frequency in the frame of reference of the medium and sees a higher index of refraction than if the medium were at rest. Conversely, the wave traveling opposite to the flow direction sees a lower index of refraction. The oscillating frequencies of the oppositely directed waves adjust themselves to maintain an integral number of wavelengths around the closed path. The wave encountering the higher index of refraction drops in frequency, and the other rises. The resultant is a beat frequency difference in the absence of rotation - i.e., drift. The drift is proportional to flow velocity times cavity loss and inversely proportional to cavity area. This flow is induced by the DC discharge and is cathode directed. Although originally called Langmuir flow, the exact mechanism is uncertain, since no model of the plasma will yield a new flow of sufficient magnitude, nor will the model even predict a cathode directed flow. Measurements of flow induced drift indicate that the flow velocity has very little current dependence, but may depend primarily on discharge potential gradient.

The bulk of the flow bias problem is handled by using a split DC discharge with a single cathode in the center of the discharge, and anodes at the extremities, and carefully balancing the gain of each half of the discharge by regulating the anode currents. It is also obviously helpful to have low optical loss in the cavity since the magnitude of flow bias is proportional to medium gain (or cavity loss).

Even with a balanced discharge, drift can be induced by a temperature gradient along the discharge, which causes a convection type of flow of the active medium. The baseline gyro incorporates a plasma tube made from single blocks of beryllia ceramic. The end-to-end thermal conductivity of the tube is several hundred times higher than the old glass-and-metal design. This, coupled with the reduction in sensitivity afforded by low cavity loss, reduces the baseline gyro tube thermal gradient problem to insignificance.

3.2.3.2 Magnetic Mirror Reversal Unbalance

The magnetic mirror is driven into saturation by an electromagnet. The current to the electromagnet is periodically reversed in order to achieve a net zero time averaged applied bias. It is evident that the positive and negative bias levels must be very highly balanced if good drift performance is to be achieved. Any unbalance results in a directly corresponding gyro drift. Fortunately, the magnetic material yields very little incremental change in bias versus applied magnetic field when the applied field is well in excess of the coercive force of the magnetic field. However, magnetic retentivity in the bias coil iron pole pieces can cause uncertainty in day-to-day drift repeatability if this retentivity varies. To eliminate this potential retentivity error, an air core magnet design is being tested. Because the magnetic mirror is a fixed phase shift device, both the body rate bias and the bias errors are inversely proportional to cavity area.

3.2.3.3 Scaling Laws For Drift Error Sources

Flow bias: The beat frequency difference developed by active medium flow is

$$\Delta f = K_f \, l \, v/p \qquad (3.5)$$

where K_f is a constant related to the gain width of the active medium, l is cavity loss (tube gain), v is average axial flow velocity, and p is cavity perimeter. Since

ring scale factor is $\Delta f = \frac{4A\Omega}{\lambda p}$ then

$$\text{Drift} = \Omega_D = \frac{\lambda p}{4A} (K_f \, 1 \, v/p) = \frac{\lambda K_f \, 1v}{4A} \tag{3.6}$$

$$\text{or Drift} = \Omega_D = \lambda K_G / p^2 \tag{3.7}$$

The above formula assumes that transport of the lasing atoms is responsible for discharge bias. Under the additional assumption that flow velocity is proportional to discharge current, doubling the cavity loss would require a doubling of current so that flow bias would be four times greater as a result. Recent experiments refute this assumption and indicate that the apparent flow velocity is more likely proportional to discharge voltage gradient, which is substantially independent of discharge current.

Magnetic Mirror Reversing Unbalance: The change in output frequency is related to the bias mirror phase-rotation according to:

$$\frac{\Delta f}{f} = \frac{\Delta \phi}{\phi_{TOT}} \tag{3.8}$$

where $\Delta\phi$ is bias mirror phase rotation and ϕ_{TOT} is the total phase change in the cavity

$$\phi_{TOT} = 2\pi N \tag{3.9}$$

where N is the integral number of wavelengths around the perimeter

$$\text{and } N = \lambda / p \tag{3.10}$$

$$\text{also } f = c/\lambda \tag{3.11}$$

Substituting into (3.8) yields:

$$\Delta f = c/p \, \frac{\Delta \phi}{2\pi} \tag{3.12}$$

The bias drift rate corresponding to this output frequency change, according to the scale-factor of the ring is:

$$\Omega_D = \frac{\lambda p}{4A} \Delta f = \frac{\lambda c}{8\pi A} \Delta \phi \tag{3.13}$$

or

$$\Omega_D = K_U \frac{\lambda \Delta \phi}{p^2} \qquad (3.14)$$

An unbalanced phase rotation causes a corresponding gyro drift.

Thus, for laser-gyro units employing the same wavelength and identical magnetic mirrors, both major drift error sources yield the following scaling-law expression:

$$\Omega_D = \frac{K_D}{p^2} \qquad (3.15)$$

There are only two measurement points available for verification of this drift repeatability scaling law: the garnet magnetic mirror 15-inch perimeter unit exhibiting 0.048 deg/hour rms (figure 3-6) and the garnet magnetic mirror 7.5-inch perimeter unit exhibiting 0.35 deg/hour rms (figure 3-2), both operating at 1.15 micron wavelength and both using similar magnetic mirrors. This ratio of 7.3 would indicate a scaling improvement with perimeter length of about $p^{-2.8}$. This empirical relationship is not too far from the theoretical p^{-2}.

3.2.4 Scale Factor Errors

The first error source in the ring laser was discovered in the first demonstration of the laser gyro at Sperry by Macek and coworkers in 1963, that of lock-in, or the disappearance of the rate signal at low rates. This phenomenon was attributed to optical backscatter coupling of the contra-rotating modes of the laser. Subsequent analysis disclosed that backscatter coupling would perturb the rate response of the laser even at rates far above lock-in. C.C. Wang at Sperry developed a comprehensive theory describing the rate characteristic in terms of two types of coupling - "skew Hermitian" and "Hermitian," these names being derived from the matrix expression for mode coupling.

In the transmission line analog of a ring resonator, skew coupling would be introduced by a resistor connected across the transmission line and Hermitian coupling by a capacitor instead of a resistor. The resistive type of coupling introduces a lock-in band and a lowering of frequency outside the lock-in band. At high rates, the measured output asymptotically approaches the ideal linear output obtained in the absence of backscatter. Resistive coupling also produces an amplitude modulation of

the two waves at the beat frequency, with the modulations of the two beams being in phase. The response characteristic is unaffected by lasing intensity.

Reactive coupling produces a markedly different rate characteristic. For a given amount of backscatter, the observed rate threshold is much less than for resistive coupling and is lasing-intensity dependent. Above lock-in, the beat frequency rises above the linear ideal and, at high rates, approaches the ideal response asymptotically. For equal coupling and high rate, the positive error created by reactive coupling is nearly equal to the negative error caused by resistive coupling. The rate at which the peak positive error occurs depends on lasing intensity. The beam modulation produced by reactive coupling is 180 degrees out-of-phase in the two beams.

Both types of coupling are normally present in a ring laser cavity. As mirror quality is improved, a shift to predominantly reactive coupling is to be expected.

Regardless of the type of coupling encountered, the achievement of stable and linear rate response demands that backscatter coupling be reduced, and that the gyro always be operated well above rate threshold by means of a biasing technique.

Nominal scale-factor error is calibrated and compensated out as is a first order variation with temperature. Scale-factor non-linearity is also calibrated and compensated as a function of measured input rates. Hence, it is only the stability and repeatability of the calibration coefficients employed that contributes to system error.

A theoretical treatise on scale-factor scaling with laser gyro perimeter has not as yet yielded a satisfactory model. Therefore, empirical data obtained on 7.5-inch and 15-inch laser gyros having the baseline design configuration is used for scaling purposes.

The empirical data used was obtained with the garnet magnetic mirror 15-inch perimeter unit (SLG-15) exhibiting 10 PPM rms scale-factor linearity, stability, and repeatability (figure 3-11) and the garnet magnetic mirror 7.5-inch perimeter unit exhibiting 64 PPM rms (figure 3-4), both operating at 1.15 micron wavelength and both

using similar magnetic-mirror phase rotation values. This ratio of 6.4 would indicate a scaling improvement with perimeter length of about $p^{-2.7}$.

Based on this data the scale-factor error (S. F. E.) follows the relationship:

$$\text{S. F. E.} = K \frac{\Omega_t^2}{\Omega_m^2} = \frac{1}{p^{2.7}}$$

where the lock-in threshold rate Ω_t of the garnet SLG-15 is about 1/10 that of the garnet SLIC-7 (0.35 deg/sec compared to 3.5 deg/sec) and the magnetic mirror bias rate Ω_m, using similar garnet magnetic mirrors, of the SLG-15 is about 1/4 that of the SLIC-7 (64 deg/sec compared to 240 deg/sec).

3.3 SCALING LAW VALIDATION

3.3.1 Baseline Gyro Performance Data (7.5-Inch Perimeter)

Sperry laser gyro performance has improved significantly with the substitution of a garnet magnetic-mirror bias element for the metallic type previously employed. An extensive on-going performance improvement program, supported by AFAL and IR&D funds, is in process.

The SLIC-7 garnet magnetic mirror unit, operating in the 1.15 micron infrared domain, exhibits a drift repeatability of 0.35 deg/hr, a white-noise random drift of 0.051 deg/$\sqrt{\text{hr}}$ rms and a scale-factor error of 64 PPM rms. The data are presented and discussed in the following paragraphs.

3.3.1.1 SLIC-7 Turn-On Bias Drift Repeatability (Including g-Sensitive Drifts)

Bias drift repeatability is the variation in the steady-state bias drift from a pre-calibrated value from turn-on to turn-on.

Figure 3-2 depicts the turn-on drift repeatability of one axis of garnet SLIC-7 S/N 003 taken over 19 days with input axis varying between horizontal (0-g) and vertical (1-g) directions. The rms drift repeatability is 0.351 deg/hour with no discernible effect of orientation.

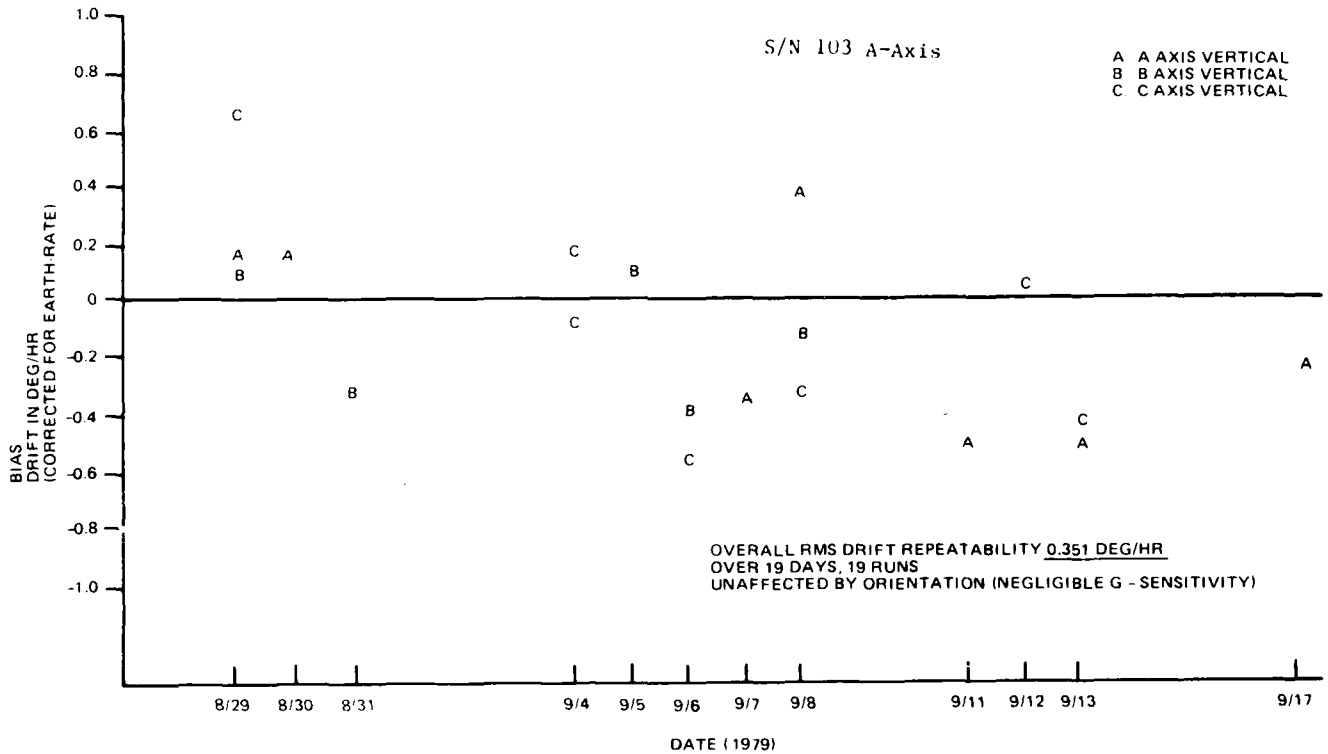

Figure 3-2. SLIC-7 (Garnet) Turn-On Drift Repeatability with Different Orientations

One of the major advantages of the laser gyro is its drift insensitivity to acceleration. This has been verified by a series of tests on various laser gyro units throughout tne years. It is confirmed again here and was also confirmed by orientation variation tests on the interim design SLIC-7 at Martin, Orlando.

3.3.1.2 SLIC-7 Random Drift

The drift rate associated with a white-noise random drift varies according to:

$$W_D = A_N/\sqrt{T}$$

where T is the sampling time of the drift angle data.

Figure 3-3 shows typical steady-state gyro drift being outputted by the present garnet SLIC-7 units. A white-noise random drift value of 0.051 deg/$\sqrt{hr}$ is observed. This is about a 2.5:1 improvement over prior metallic bias mirror units, while utilizing a magnetic mirror bias value (280 deg/sec) that is 2.8 times as large as the metallic units.

3.3.1.3 SLIC-7 Scale-Factor Repeatability/Linearity

Figure 3-4 presents scale-factor repeatability and linearity data taken on a garnet SLIC-7 unit, covering an input rate range of 3 deg/sec to 600 deg/sec, over one week of time with off-periods of days between runs. The overall rms deviation is observed to be 64 PPM (0.0064%) of the input rate. This is about a 3:1 improvement compared to prior metallic bias mirror units.

3.3.1.4 SLIC-7 Scale-Factor Turn-On Transient

A run was performed on a garnet SLIC-7 to determine scale-factor performance transient behavior from a cold start. Figure 3-5 presents the results obtained. These data were uncompensated (actual systems measure gyro temperature and incorporate a scale-factor temperature coefficient correction). A scale-factor measurement at 20 deg/sec was performed every 36 seconds.

Even without compensation the scale-factor error at a 20 deg/sec input rate is observed to be always less than about 200 PPM (0.02%) of the input rate (less than 100 PPM after the first 10 minutes).

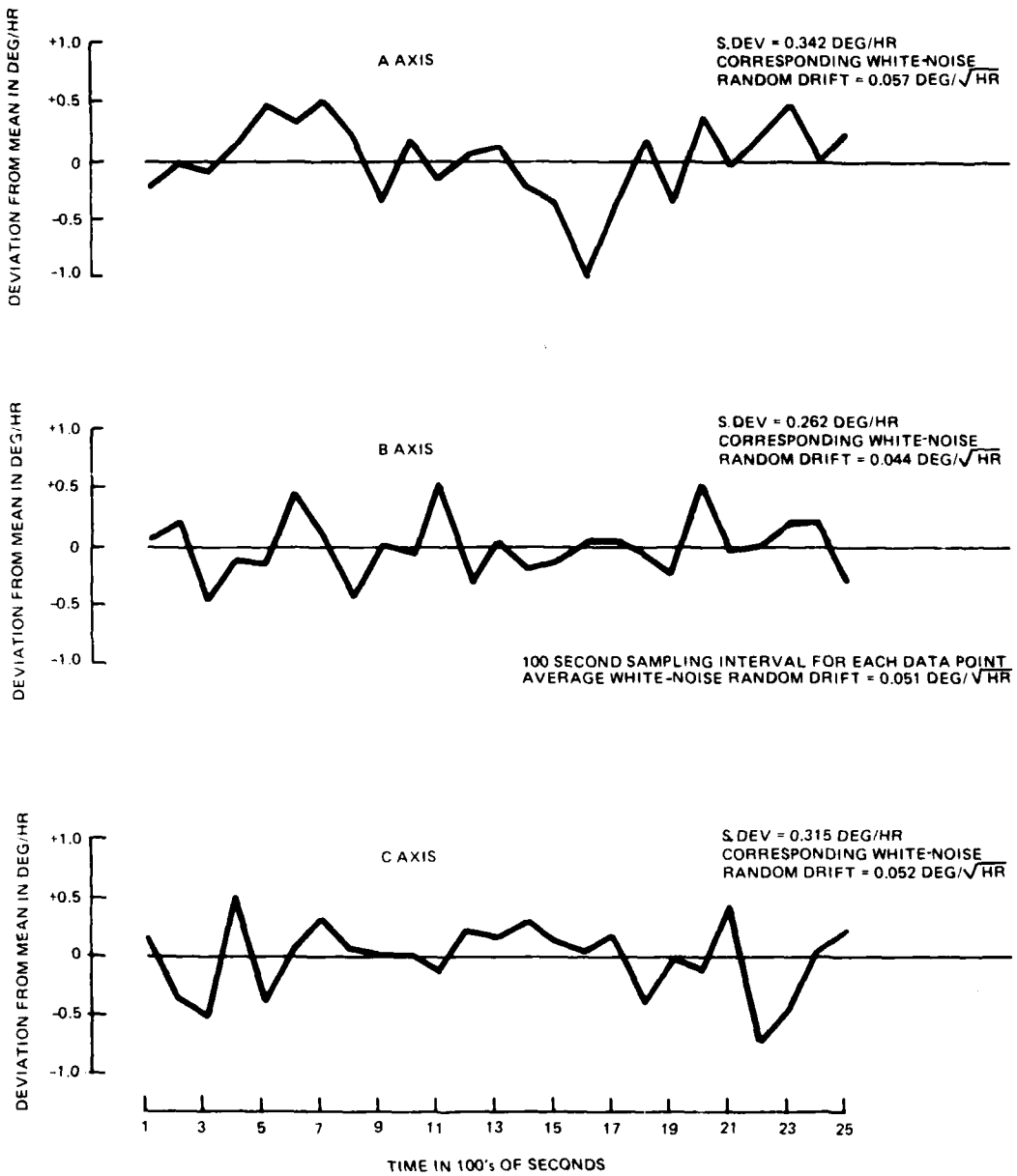

Figure 3-3. SLIC-7 (Garnet) S/N 102 Steady State Gyro Drift

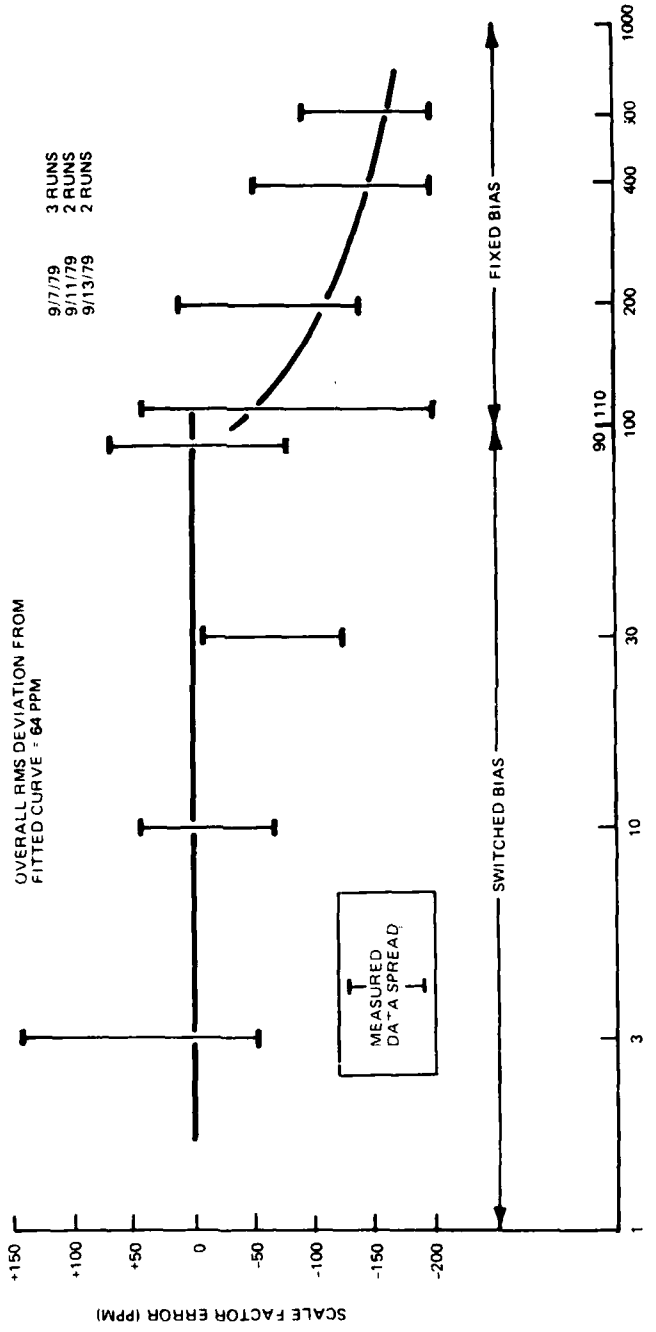

Figure 3-4. SLIC-7 (Garnet) Scale Factor Linearity/Repeatability (S/N 103 A-Axis)

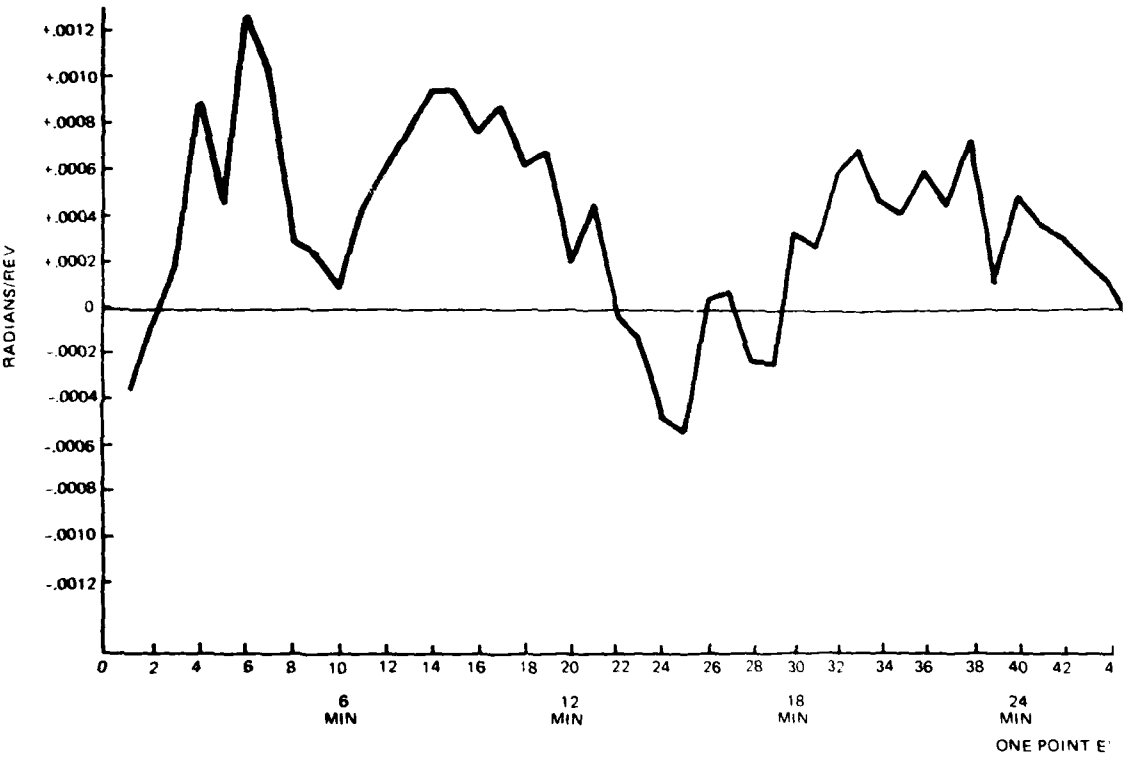
RADIANS/REV
+.0012
+.0010
+.0008
+.0006
+.0004
+.0002
0
-.0002
-.0004
-.0006
-.0008
-.0010
-.0012
0 2 4 6 8 10 12 14 16 18 20 22 24 26 28 30 32 34 36 38 40 42 4
6 MIN
12 MIN
18 MIN
24 MIN
ONE POINT E

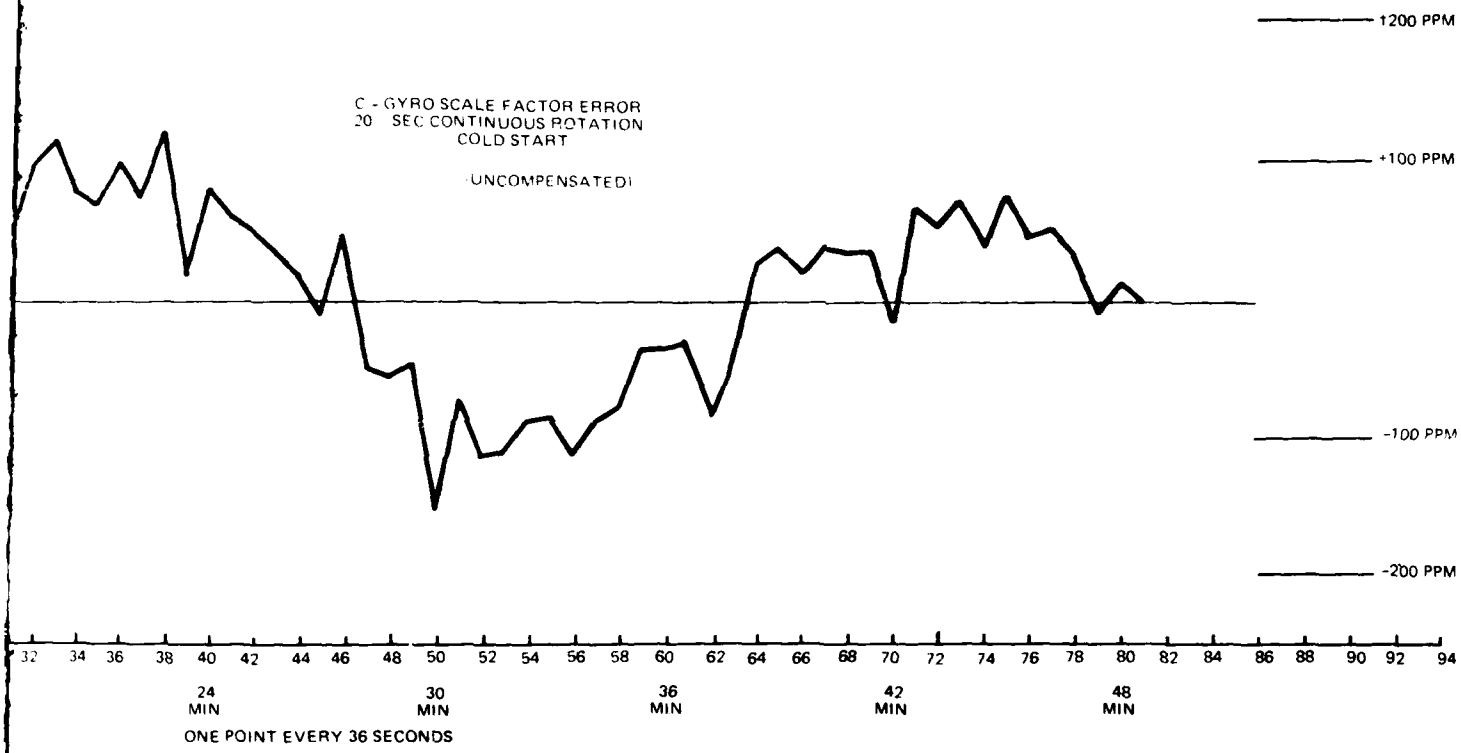

Figure 3-5. SLIC-7 (Garnet) Scale Factor Turn On Transient

3.3.2 SLG-15 Gyro Performance Data (15-Inch Perimeter)

The SLG-15 garnet magnetic-mirror unit, operating in the 1.15 micron infrared domain, exhibits a drift repeatability of 0.048 deg/hr, a white-noise random drift of 0.011 deg/$\sqrt{\text{hr}}$ rms and a scale-factor error of about 10 PPM rms. The data presented in figures 3-6 through 3-10 show typical drift rate plots and also demonstrate that the random drift is indeed white-noise. The data presented in figure 3-11 shows scale-factor repeatability (day-to-day), stability (run-to-run on a given day), and linearity (different input rates) to be within 10 PPM rms.

3.3.3 SLG-21 Gyro Performance Data (21-Inch Perimeter)

A single SLG-21 garnet magnetic mirror unit, operating in the 1.15 micron infrared domain, was assembled to verify the white-noise random drift scaling law with perimeter length. Figure 3-12 depicts a 33 hour stretch of steady-state drift rate data (bias drift removed) taken on this unit in a laboratory environment (room temperature variations). The data are uncompensated. Random drift analysis over the flat portion from 8 to 13 hours yields a white-noise random drift of 0.0056 deg/$\sqrt{\text{hr}}$. This is in exact agreement with the scaling law prediction, in comparison with the SLG-15, if 0.011 deg/$\sqrt{\text{hr}}$ is taken to be typical of the SLG-15 garnet units:

$$\left(\frac{15}{21}\right)^2 \times 0.011 = 0.0056$$

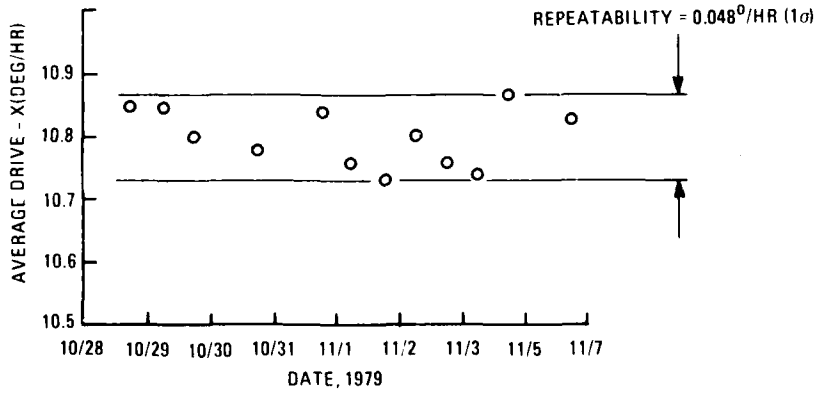

Figure 3-6. SLG-15 Garnet Mirror Gyro G6
Drift Rate Repeatability (Uncompensated)

3.4 PERFORMANCE RANGE DESIGNS

The statement of work specifies that an analysis of the performance/cost range potential of the baseline gyro be made. The ground rules for this analysis state that the generic design of the baseline gyro be adhered to. This essentially establishes that size be the dominant performance trade off parameter. The foregoing section establishes the performance scaling laws based on optical perimeter length. Table 3-4 lists the required performance ranges for the three key performance parameters: bias uncertainty, random drift, and scale factor. In addition, the scaling laws and baseline gyro performance are noted.

This data was used to analyze the high performance requirements.

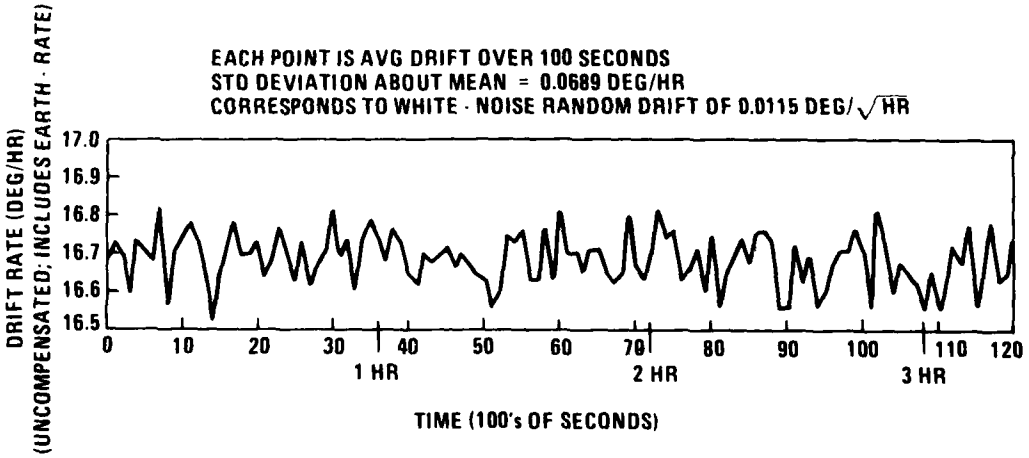

Figure 3-7. SLG-15 (Garnet) Magnetic Mirror Gyro Drift Rate

TIME(HRS)	MEAN DRIFT OVER HOUR (DEG/HR)	STANDARD DEVIATION ABOUT MEAN (100-SECOND SAMPLES) (DEG/HR)
1	16.6997	.0655
2	16.6867	.0557
3	16.6761	.0740
4	16.6708	.0765
5	16.6817	.0690
6	16.6686	.0716
7	16.6739	.0673
8	16.6961	.0687
9	16.6925	.0724
10	16.6856	.0666
MEAN OF MEANS	16.6832	RMS OF S.D.'s .0689
STD DEV OF MEANS (Equiv to 1 HR sample time)	.0108	

Figure 3-8. One-Hour Drift Analysis of Figure 3-7 Data

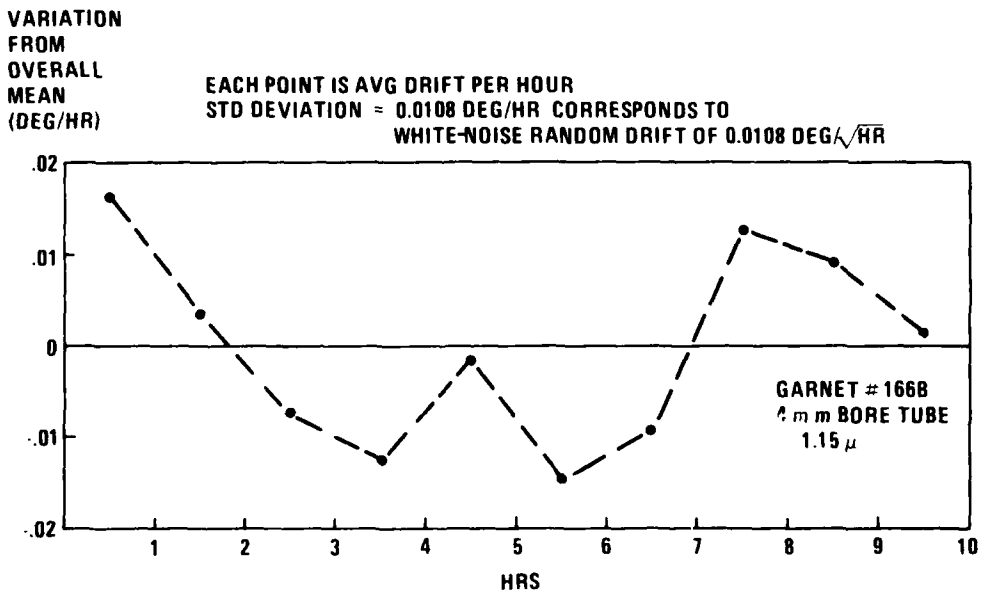

Figure 3-9. SLG-15 (Garnet) Magnetic Mirror Gyro Bias Stability over 10 Hours

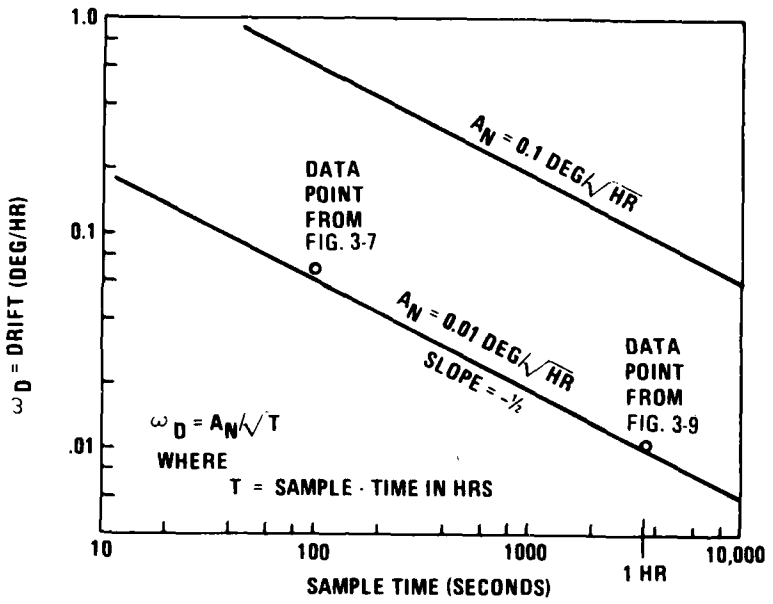

Figure 3-10. White Noise Random Drift Vs Sample Time

INPUT/DATE (1979) RATE	3/28	3/29	3/30	4/2	4/3	GARNET BIAS MIRROR SLG-15 S/N 009
10 DEG/SEC	829 591	581	589	590	599	MEAN:
	595	586	596	599	580	829591
	594	584	596	602	594	S.D.: 7.1
	589	580	588	602	592	= 8.6 PPM
	579				596	
20 DEG/SEC	588	586	584	590	601	MEAN:
	594	588	601	605	583	829593
	598	586	600	606	593	S.D.: 7.0
	587	589	593	603	593	= 8.4 PPM
	588				592	
40 DEG/SEC	593	586	591	603	604	MEAN:
	594	587	606	613	592	829597
	605	591	596	614	590	S.D.: 9.1
	591	586	599	616	598	= 11 PPM
	593				593	
						OVERALL RMS DEVIATION = 9.4 PPM

Figure 3-11. Scale Factor Repeatability, Stability, Linearity

3.4.1 High Performance SLIC-22

To satisfy all the high performance characteristics (0.005 deg/$\sqrt{\text{hr}}$ white-noise random drift, 0.02 deg/hr drift repeatability, and 20 PPM scale-factor error), about a 22.5-inch perimeter gyro is required. The white-noise random drift of a 21-inch unit has already been measured close to the desired value and the scale-factor error of a 15-inch unit has already been measured to be about 50 percent of that required. Applying the scaling laws to the SLIC-7, SLG-15, and SLG-21 data shows that the SLIC-22 will satisfy the high performance requirements. In making the transition from the SLIC-7 to the SLIC-22, size is the only trade-off. Therefore, to the first order, the cost of each sensor would be the same (a characteristic of the laser gyro where cost is essentially uncoupled from performance).

However, there are some cost increases associated with this high performance unit. The optical assembly is bigger and raw material costs would be higher. In addition, yield on optical components would be lower (acceptance limits tighter to achieve a high sensor yield) and increased test time would be needed. An analysis was made of the baseline gyro costs to estimate the increase associated with the SLIC-22 production. This analysis showed an approximate 10% increase in cost for the SLIC-22 (the electronics assembly would be unchanged). This results in a three-axis cost of approximately $14,000 ($4667/axis).

3.4.2 Low Performance SLIC-7 (Modified)

To satisfy the low performance end of the spectrum (1 deg/$\sqrt{\text{hr}}$ random drift, 3.0 deg/hr repeatability, and 500 PPM scale-factor error), one could conceive of a SLIC-3 miniature laser gyro having a 3-inch perimeter. However, practical considerations (tube design, etc.) tend to keep the smallest perimeter close to that of the baseline SLIC-7. Some cost savings could accrue by relaxing specifications on mirror and tube quality (or use rejected elements from higher performance units), minimizing alignment optimization time, maximizing yield (less recycling of elements), and reducing test time.

An analysis of the detailed cost data presented in Appendix A on the baseline gyro was made to eliminate some of its performance enhancing elements. Extra magnetic shields, mirror clamping devices, light absorbers and yields were considered. In addition, a reduction in test and engineering was made with

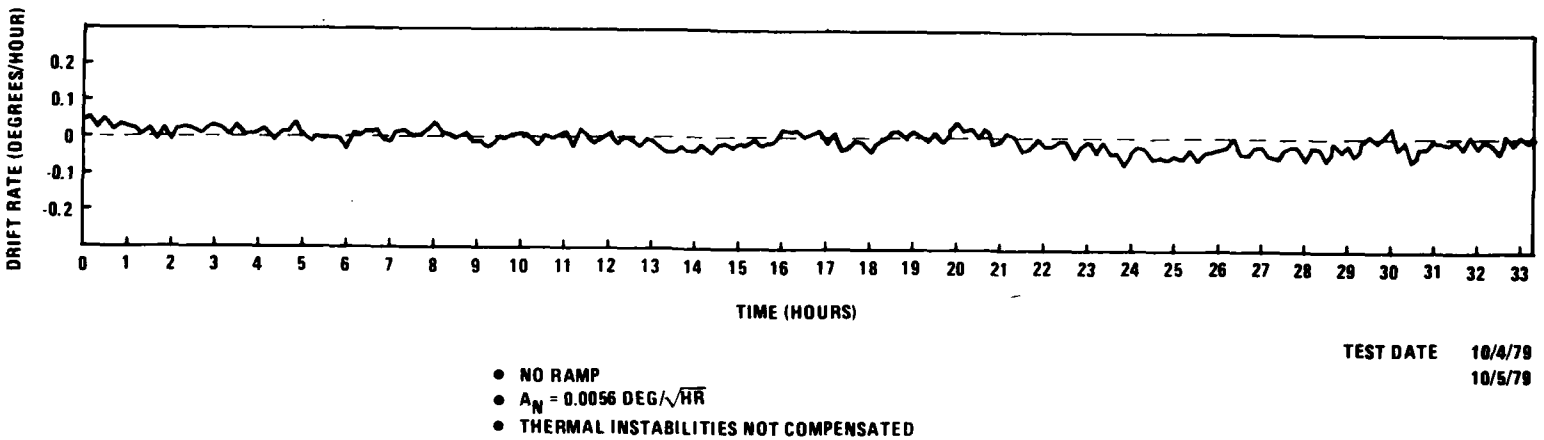

Figure 3-12. SLG-21 (Garnet) Magnetic Mirror Gyro Uncompensated Bias Stability Over 30 Hours

Table 3-4. Key Performance Parameters

Performance Parameter	Scaling Law	Required Range	Baseline P = 7.5 inch
Bias uncertainty °/HR	$\frac{1}{P^{2.8}}$	0.02 to 3.0	0.5
Random drift °/$\sqrt{HR}$	$\frac{1}{P^{2}}$	0.005 to 1.0	0.05
Scale factor error PPM	$\frac{1}{P^{2.7}}$	20 to 500	100

the overall result presented in table 3-5. Comparing this cost estimate to that presented in section 2-3 shows that nearly a 20% reduction is attainable. This provides a per axis cost of approximately $3500.

3.4.3 Cost-Performance - Size Tradeoff

Figures 3-13 and 3-14 present tradeoff information relating to performance, cost, and size that reflect the possible design extrapolations to cover the specified range. White-noise random drift is employed as the performance comparison factor as this is the most important parameter in many missile applications. A cylindrical shape gyro sensor package is assumed for all units.

It is observed that cost versus performance is a fairly flat characteristic since random drift performance improves as $1/p^2$, using similar laser-gyro elements.

3.4.4 Generic Design Performance Improvement

For performance in the high performance end of the spectrum (and beyond) continued size increase is not an attractive alternative. Therefore, Sperry has been investigating a modification to the baseline design that could be considered within the generic configuration. This involves converting from the infrared wavelength to the visible red wavelength. Performance improvements of an order of magnitude are postulated for comparable size gyros. What this means is that the random drift performance of the SLIC-22 would be improved to 0.0005 °/$\sqrt{HR}$. Or conversely, the size could be reduced to the 7.5-inch perimeter to achieve the high performance

end of the missile grade range of 0.005 °/$\sqrt{HR}$. However, the modular construction with the garnet mirror imposes a finite limit on size reduction due to the tube discharge length restriction (available gain to overcome loss) associated with a single leg of the optical path.

Currently a modular, visible red wavelength, garnet biased laser gyro is operating in a 21-inch perimeter. This configuration is being optimized to establish an important data point to validate the postulated 10:1 improvement factor.

Table 3-5. Simplified SLIC-7 Cost Estimate
(1978 Dollars, 16% G&A, 10% Fee)

	Sensor Ass'y	Electronics Ass'y
Material	3344	3029
Machining	539	119
Assembly	968	442
Inspection and test	669	157
Engineering and quality control	979	256
	$ 6499	$ 4003
Total Unit Cost	$10,502	
Per Axis Cost	$ 3,500	

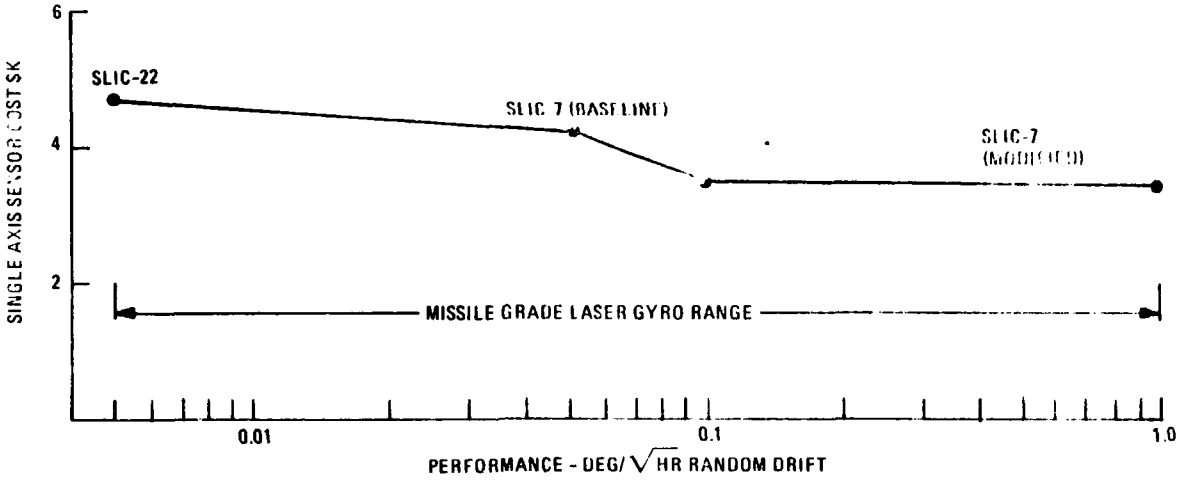

Figure 3-13. Cost Vs Performance Range

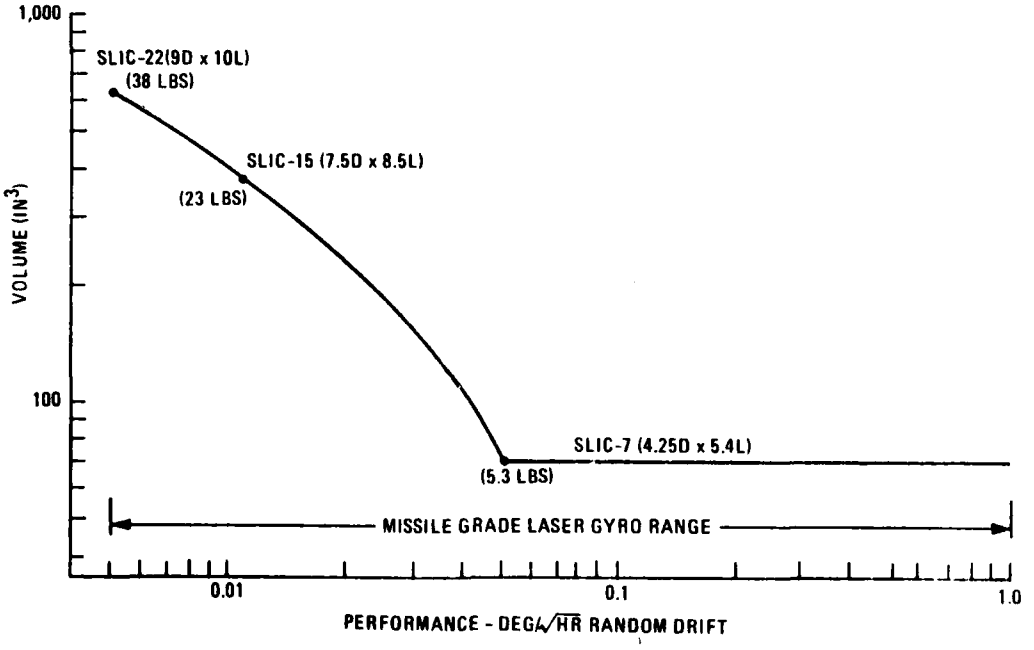

Figure 3-14. Size Vs Performance Range

Appendix A

BASELINE GYRO COST ESTIMATE

This appendix contains the detailed material, machining and assembly cost breakdown relative to producing a quantity of 700 baseline gyros at a 30 per month production rate. The estimates presented are based on Sperry predictions where the baseline gyro will be produced in a high volume production facility currently being planned. The data presented in this appendix is the result of an intensive in-house producibility effort that has been on-going during the duration of the Joint Service Phase I program. Estimates are continually updated to reflect the results of cost reducing inputs. 1979 dollars are the base for this in-house program. Therefore, to satisfy the statement of work requirement for generating the baseline gyro costs in 1978 dollars, the 1979 estimates have been reduced by 8.5% to adjust for the 1978 to 1979 inflation rate. (Note: the 8.5% is an average of Sperry's actual experience).

The estimates presented include a general and administrative (G&A) adjustment of 16% and a fee of 10%.

The baseline gyro (Sperry Model SLIC-7) consists of two separate assemblies: a Sensor Assembly and an Electronics Assembly. The Sensor Assembly, part number 6077074, houses the optics required for three axes of laser gyro rate sensing. The Electronics Assembly, part number 6077072, contains the circuit boards and power supply necessary for the three axis laser gyro system to function.

Figure A-1 shows the cost breakdown for the sensor assembly and the electronics assembly by major subassembly. The detailed labor and material breakdown for each assembly is presented in tables A-1 (Sensor Assembly) and A-2 (Electronics Assembly). These estimates are at the manufacturing cost line and are multiplied by 16% G&A and 10% fee to get the costs quoted in figure A-1.

It should be noted that the costs presented are based on a three-axis configuration. Therefore, to get a comparable single-axis cost, these estimates should be divided by three. The per axis cost is estimated to be $4238.

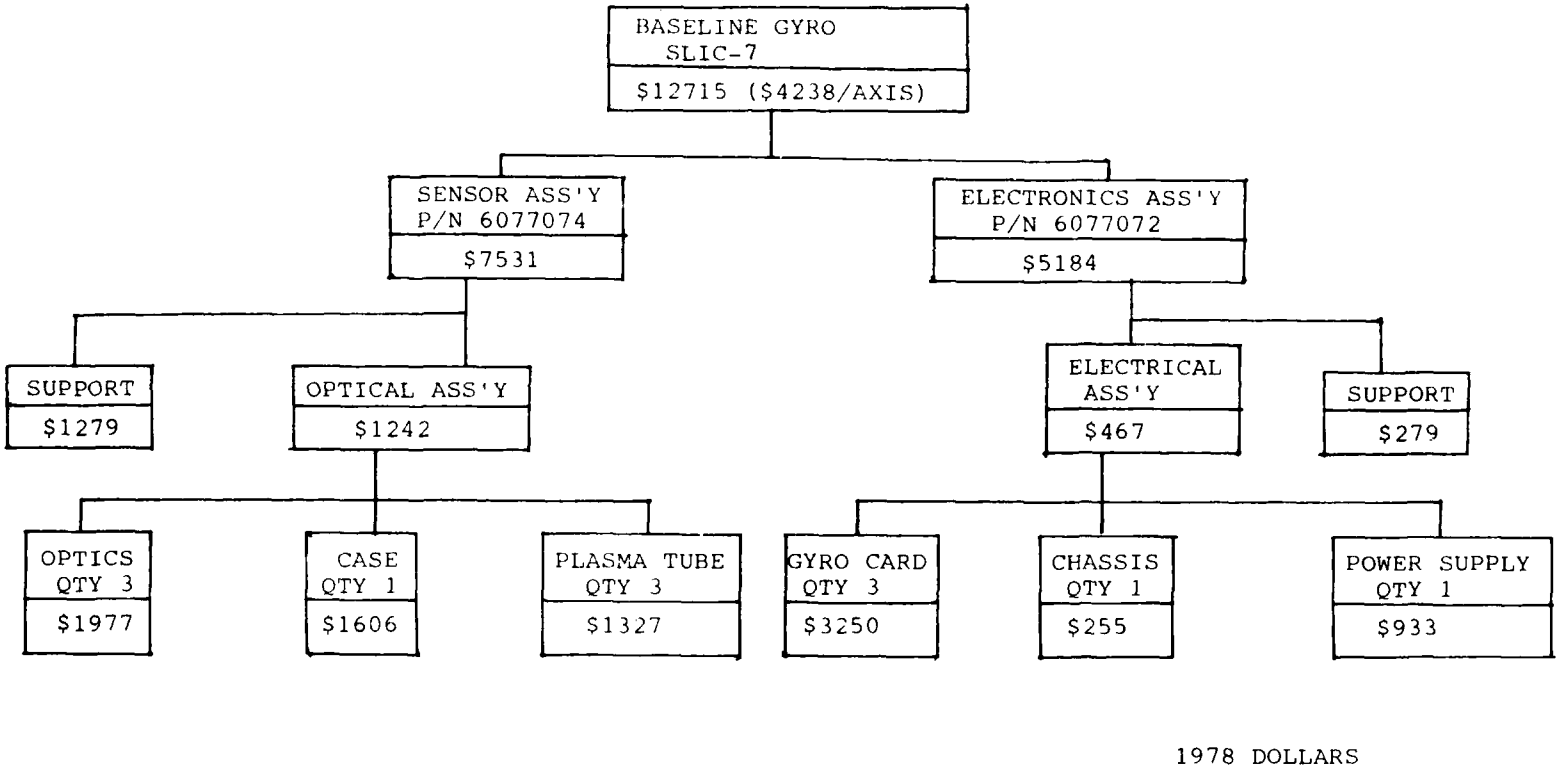

Figure A-1. Baseline Gyro Cost Breakdown by Major Assembly

TABLE A–1
ASSEMBLY BREAKDOWN SHEET and/or SUMMARY
(SENSOR ASSEMBLY)

PART NUMBER	DESCRIPTION	QTY	MATERIAL $ UNIT	MATERIAL $ TOTAL	REMARKS	MACHINING (HRS) SETUP	MACHINING (HRS) UNIT LABOR	MACHINING (HRS) TOTAL LABOR	ASSEMBLY (HRS) SETUP	ASSEMBLY (HRS) UNIT LABOR	ASSEMBLY (HRS) TOTAL LABOR
Sub Ass'y A	Bobbin Ass'y	3									
6050607	Bobbin	2	14.75	29.50						0.42	0.89
6025870	Washer	2	0.04	0.08							
W5788136000	Wire	A/R			1500 Ft Spool						
	ADH 26	A/R									
	Tape	A/R									
				29.58							0.84
				X 3							X 3
	Total			88.74							2.52
Sub Ass'y B	Bias Coil Ass'y	3									
6050612	Flux Ret. Plate	1	4.38	4.38							0.63
6000954-2	Terminal	4	0.11	0.44							
	ADH 26	A/R									
6050674	Stud Bias	2	0.50	1.00							
6025870	Washer	2	0.02	0.04							
0164-3	L'washer	2	0.04	0.08							
0424-4	Nut	2	0.08	0.16							
6000940	Pin	2	0.08	0.16							
2932232	Shrink Sleeve	2"									
	Wire(26AWG) Wht	24"									
				6.26							0.63
				X 3							X 3
	Total			18.78							1.89
Sub Ass'y C	Bias Coil & Temp. Sensor Ass'y	1									0.21
6000940	Pin	2	0.08	0.16							
6025940	Bracket Temp. Sens.	1	0.89	0.84							
6000954-3	Terminal	2	0.11	0.22							
6000942	Temp. Sensor	1	11.30	11.30							
	ADH 26	A/R									
	Wire (26 AWG) Wht										
2933252	Shrink Sleeve	2"									
	Total			12.52							0.21
Sub. Ass'y D	Mtg. Plate Ass'y	3									0.63
6050296	Mtg. Plate	1	0.50	0.50		9.80	0.37	0.37			
6000954-2	Terminal	2	0.11	0.22							
	ADH-26	A/R									
				0.72				0.37			
				X 3				X 3			
	Total			2.16		9.80		1.11			0.63

TABLE A-1
ASSEMBLY BREAKDOWN SHEET and/or SUMMARY
(SENSOR ASSEMBLY) (CONT'D)

PART NUMBER	DESCRIPTION	QTY	MATERIAL $ UNIT	MATERIAL $ TOTAL	REMARKS	MACHINING (HRS) SETUP	MACHINING (HRS) UNIT LABOR	MACHINING (HRS) TOTAL LABOR	ASSEMBLY (HRS) SETUP	ASSEMBLY (HRS) UNIT LABOR	ASSEMBLY (HRS) TOTAL LABOR
Sub Ass'y E	Piezo & Actuator Bridge Ass'y	3								2.43	7.29
4331-501411-1	Piezo Elec.-Outer	1	12.90	12.90							
4331-501411-2	Piezo Elec.-Inner	1	12.06	12.06							
6000464	Mirror Piezo	1	77.70	77.70							
W-5783136-000	Wire, Form Var	A/R									
	ACME Solder #302.1	A/R									
	ADH 28	A/R									
6000940	Pin	2	0.17	0.34							
2932232	Shrink Sleeve	A/R									
	Wire (26 AWG) Brn	12"									
4331-302189	Actuator Bridge	1	4.20	4.20							
	ADH 26	A/R									
	Wire (26 AWG) Wht	12"									
				107.20 X 3							
	Total			321.60							7.29
Sub Ass'y F	Conn. Ass'y	1									9.11
6000955	Connector	1	22.32	22.32							
	Wire (26 AWG) Wht	84"									
	Wire (26 AWG) Brn	36"									
	Wire (26 AWG) Grn	24"									
	Wire (26 AWG) Shield Wht	36"									
	Wire (26 AWG) Orn	36"									
	Wire (26 AWG) Vio	12"									
	Wire (26 AWG) Yel	12"									
	Wire (26 AWG) Red	48"									
	Wire (24 AWG) Blk	12"									
	Total			22.32							9.11
Sub Ass'y G	Resistor Plate Ass'y	1									0.84
6025859	Resistor Plate	1	1.98	1.98							
6000950-2	Resistor (15K)	3	3.34	10.02							
6000950-2	Resistor (41S)	1	3.50	3.50							
	ADH 26	A/R									
	Wire (26 AWG) Insulated Buss	12"									
	Wht	12"									
	Grn	12"									
	Total			15.50							0.84

TABLE A–1
ASSEMBLY BREAKDOWN SHEET and/or SUMMARY
(SENSOR ASSEMBLY) (CONT'D)

PART NUMBER	DESCRIPTION	QTY	MATERIAL $ UNIT	MATERIAL $ TOTAL	REMARKS	MACHINING (HRS) SETUP	MACHINING (HRS) UNIT LABOR	MACHINING (HRS) TOTAL LABOR	ASSEMBLY (HRS) SETUP	ASSEMBLY (HRS) UNIT LABOR	ASSEMBLY (HRS) TOTAL LABOR
Sub Ass'y H	Base Plate Ass'y (Mech)	1									
6076880	Bottom Plate	1	5.05	5.05		38.12		2.42			
0919-14	Screws	4	0.04	0.16							
6050842	Studs	2	0.57	1.14							
	ADH 26	A/R									
6000956	Resistors	6	3.21	19.26							
	Wire (24 AWG)										
	Bare Buss	6"									
	Shrink Sleeve	12"									
	Shrink Sleeve	6"									
6077570	Resistor Holder	1	0.44	0.44		15.08		4.69			1.68
0919-7	Screws	2	0.04	0.08							
	ADH 26	A/R									
	RTV-11 Compound	A/R									
6025027	Terminals	4	0.12	0.48							
2920617000	Polyimide Plastic Sheet	6 in^2									
6000954-1	Terminal	9	0.57	5.13							
	Total			31.74		53.20		7.11			1.68
Sub Ass'y I	Base Ass'y (Wiring)	1									3.77
5704724-001	Wire (Hi-Volt) Blk	36"									
-010	Wire (Hi-Volt) Wht	36"									
-007	Wire (Hi-Volt) Blue	36"									
2932232-02500	Shrink Sleeve	18"									
6000952-1	"O"-Ring	1	0.34	0.34							
610327800-000	Vacuum Compound	A/R									
6000462	Vacuum Gage	1	28.20	28.20							
	ADH 26	A/R									
6000942	Temp. Sensor	1	11.30	11.30							
5704626-005	Wire (26 AWG) Yel	48"									
-010	Wire (26 AWG) Wht	48"									
-006	Wire (26 AWG) Grn	24"									
6076098	Pre Amp Ass'y	3	71.40	214.20							
	Lacing Cord	A/R									
0919-2	Screws	6	0.04	0.24							
6000953	Lug	2	0.02	0.04							
0919-1	Screw	2	0.04	0.08							
	L'washer	2	0.04	0.08							
5704626-001	Wire (26 AWG) Blk	72"									
	Shielded Wire	72"									

(CONTINUED)

TABLE A–1
ASSEMBLY BREAKDOWN SHEET and/or SUMMARY
(SENSOR ASSEMBLY) (CONT'D)

PART NUMBER	DESCRIPTION	QTY	MATERIAL $ UNIT	MATERIAL $ TOTAL	REMARKS	MACHINING (HRS) SETUP	MACHINING (HRS) UNIT LABOR	MACHINING (HRS) TOTAL LABOR	ASSEMBLY (HRS) SETUP	ASSEMBLY (HRS) UNIT LABOR	ASSEMBLY (HRS) TOTAL LABOR
5704626	Wire (26 AWG) Brn	24"									
6050326	Pin, Alignment	2	2.84	5.68							
6076877	Shield Ass'y Outer (Bottom Only)	1	13.50	13.50							
6075696	Spacer	1	0.22	0.22		5.20		0.12			
6076976	Shield Ass'y Middle (Bottom Only)	1	13.49	13.49							
0919-3	Screw	3	0.04	0.12							
6076882	Shaft	1	3.88	3.88							
0923-1	Set Screw	2	0.04	0.08							
MS27491-22D	Socket	36	0.08	2.88							
2932232	Shrink Sleeve	48"									
	Total			294.33		5.20		0.12			3.77
Sub Ass'y J	Photo Diode Ass'y	3								0.84	2.52
4331-302194	Photo Diode Ass'y	1	30.46	30.46							
5706026-010	Wire (26 AWG) Shield	6"									
57046026-001	Wire (26 AWG) Blk	2"									
2934032-02500	Shrink Sleeve	1"									
	ADH 26	A/R									
6050256	Light Absorber Bkt	1	1.88	1.88							
6025199	Light Absorber	1	0.60	0.60							
6050254	Output Mirror Bkt	1	0.12	0.12		2.80		0.34			
6050255	Detector Bkt	1	1.58	1.58							
	Screw	2	0.04	0.08							
				34.72 X 3							
	Total			104.16		2.80		1.02			2.52
Sub Ass'y K	Bracket & Temp Senor	1									0.21
6025941	Bracket	1	0.83	0.83							
6000954-3	Terminal	2	0.11	0.22							
	ADH 26	A/R									
6000942	Temp. Sensor	1	11.16	11.16							
6000940	Pin	2	0.08	0.16							
	Shrink Sleeve	2"									
	Total			12.37							0.21

TABLE A–1
ASSEMBLY BREAKDOWN SHEET and/or SUMMARY
(SENSOR ASSEMBLY) (CONT'D)

PART NUMBER	DESCRIPTION	QTY	MATERIAL $ UNIT	MATERIAL $ TOTAL	REMARKS	MACHINING (HRS) SETUP	MACHINING (HRS) UNIT LABOR	MACHINING (HRS) TOTAL LABOR	ASSEMBLY (HRS) SETUP	ASSEMBLY (HRS) UNIT LABOR	ASSEMBLY (HRS) TOTAL LABOR
		1									
Sub Ass'y L	Cavity Preparation Ass'y	1									2.51
6076982	Cavity	1	75.53	75.53		0.73		19.56			
054-044	Pin-Piezo	3	0.25	0.75							
6025928	Nut Barrel-Tube	6	0.47	2.82							
0812-12	Screw	1	0.04	0.04							
0819-TBA	Screw (4-40X.625L)	11	0.04	0.44							
6025538	Nut Barrel	18	0.25	4.50							
0819-5	Screws (2-56 x 5/8)	6	0.04	0.24							
6025558	Nut Barrel	3	0.47	1.41							
6050671	Stud Bias	6	0.50	3.00							
6025929-1	Stud	6	0.50	3.00							
6025929-2	Stud	3	0.50	1.50							
	ADH 26	A/R									
	Total			93.23		0.73		19.56			2.51
6077074											
Sub Ass'y M	RLG Mech Ass'y										33.10
6076883	Base Plate	1	2.91	2.91							
0770-3	Washer, Flat	9	0.04	0.36							
6000945-1	Washer, Spring	6	0.17	1.02							
0424-4	Nut	9	0.04	0.36							
6050327	Adapter "O" Ring	1	1.33	1.33							
6000952-2	"O" Ring	1	0.07	0.07							
610327800	Silicone Compound	A/R									
0819-5	Screws	6	0.04	0.24							
6000945-1	Washer, Spring	12	0.02	0.24							
6050257	Spring	6	1.25	7.50							
0819-261	Screw	6	0.04	0.24							
6077002	Cradle Guide	6	4.15	24.90							
0819-TBA	Screw(4-40 x .625L)	11	0.04	0.44							
0819-12	Screw	1	0.04	0.04							
6000945-1	Washer, Spring	24	0.17	4.08							
6077123	Tube Ass'y	3	319.30	957.90		12.46	1.13	3.39		5.45	16.35
6050731-2	Tube Shim	12	0.25	3.00							
6050670-3	Tube Shim	3	0.75	2.25							
0819-10	Screw	12	0.04	0.48							
6050671	Stud, Bias	6	0.83	4.98							
6050672	Spacer, Bias	6	0.75	4.50							
6000945-1	Washer, Spring	12	0.17	2.04							
0424-2	Nut	6	0.04	0.24							
6050698	Pole Shoe	6	2.41	14.46							

TABLE A–1
ASSEMBLY BREAKDOWN SHEET and/or SUMMARY
(SENSOR ASSEMBLY) (CONT'D)

PART NUMBER	DESCRIPTION	QTY	MATERIAL $ UNIT	MATERIAL $ TOTAL	REMARKS	MACHINING (HRS) SETUP	MACHINING (HRS) UNIT LABOR	MACHINING (HRS) TOTAL LABOR	ASSEMBLY (HRS) SETUP	ASSEMBLY (HRS) UNIT LABOR	ASSEMBLY (HRS) TOTAL LABOR
	ADH 26	A/R									
6000463	Mirror Output	3	76.78	230.34							
6050773	Holder Bias Mirror	3	1.58	4.74							
6050792	Bias Coil Stud	3	0.83	2.49							
6000952	Spring Bias Mirror	3	1.41	4.23							
6050658	Plate Spring	3	0.17	0.51							
0183-4	Ring Retainer	3	0.04	0.12							
6050731-1	Tube Shim (Select)	3									
-3	Tube Shim (Select)	3									
6050670-1	Tube Shim (Select)	3									
-2	Tube Shim (Select)	3									
-4	Tube Shim (Select)	3									
-5	Tube Shim (Select)	3									
6025927	Magnet Mirror (Garnet)	3	110.06	330.18							
6050002	Prism	6	34.03	204.18							
6050023	Prism Ass'y	3				0.05	0.98	2.94			
	Total			1810.37		12.96		6.33			49.45
Sub Ass'y N	Final Ass'y										8.37
6000952-1	"O" Ring	1	0.33	0.33							
0327800-000	Silicone Compound	A/R									
6050610	Nut, Cavity	1	12.44	12.44							
6000951	Washer, Spring	1	0.14	0.14							
6077082	Upper Mtg Plate	1	4.90	4.90							
6000952-2	"O" Ring	1	0.07	0.07							
	ADH 26	A/R									
6076876	Shield Ass'y Middle (Top)	1									
6075698	Spacer Small (Upper)	1	0.04	0.04							
6076877	Shield Ass'y Outer (Top)	1									
6050634	Shim Case	1	0.15	0.15							
6076881	Case Outer	1	30.50	30.50		26.80	2.59	2.59			
6000952-4	"O" Ring	1	0.33	0.33							
6050609	Nut Clamping	1	6.13	6.13							
6000952-3	"O" Ring	1	0.07	0.07							
6050320	Plate Seal	1	0.12	0.12		6.40	0.22	0.22			
0920-2	Screw	8	0.04	0.32							
6000952-1	"O" Ring	1	0.08	0.08							
0819-4	Screw	2	0.04	0.08							
4331-302185	Cap Pinch-Off	1	0.45	0.45							
6077177	Name Plate	1	0.21	0.21							
6050319	Pinch-Off Tube Ass'y	1	8.81	8.81							
	Total			65.19		33.20		2.81			8.37
Totals For Each System				2893.01		117.89		38.08			91.00

TABLE A-2
ASSEMBLY BREAKDOWN SHEET and/or SUMMARY
(ELECTRONICS)

PART NUMBER	DESCRIPTION	QTY	MATERIAL ($) UNIT	MATERIAL ($) TOTAL	REMARKS	MACHINING (HRS) SETUP	MACHINING (HRS) UNIT LABOR	MACHINING (HRS) TOTAL LABOR	ASSEMBLY (HRS) SETUP	ASSEMBLY (HRS) UNIT LABOR	ASSEMBLY (HRS) TOTAL LABOR
6077072	Elec. Assy	–									27.72
6077096	Board, Resist.	1		1.16		10.61		0.51			
6077097	Chassis	1		2.48		19.02		0.82			
6077065	Cover, Rear	1		5.38		32.36		0.97			
6077066	Cover, Top	2		4.32		8.02		0.32			
6077049	Gyro Elect. Cards	3									
WTB44SEO 1154370-1	Connector	3		32.73							
Caddock MS260 N	Resistor	3		6.54							
	Misc. Parts					18.87		0.85			5.58
6025924	Term. Comp.	6		0.78							
6077049	Gyro Card	(3)								1.46	4.38
6077112	Heat Sink Dwb.	1		11.49		8.28	0.72	2.16			
4283-00880	Path Leng. Hyb.	1		372.79							
4283-00879	Bias Reg. Hyb.	1		95.86							
4283-00867	Disch Reg Hyb.	1		139.91	These Totals						
4282-01142	Ref. Hybrid	1		102.25	For 1 Card.						
T1 3ST1-2	Oven	1		4.80	3 Cards Are						
1N4891 A	Diode	1		15.34	Shown In						
1N6092	L.G.D.	1		4.74	Final Total.						
M5220.N	Resistor	2		4.84	Set-Up Is						
54LS00	Micro/^{0}K	1		0.82	Unchanged.						
1202608	Resistor	10		2.00							
6050707	Wedge Lock	2		4.70							
336658-6	Stand Off	4		0.32							
339351-39	Capacitor	1		0.56							
339067-14	Capacitor	1		1.65	These Totals						
632638-206	Diode	1		0.41	Are For 1 Card.						
AIRBN WT844 PR754929-1	Connector	1		6.29	3 Cards Are Shown In						
339065-90	Resistor	2		0.82	Final Total.						
Technetics	Power Supply	1		819.40							
	Total			3181.56		97.16		5.63			37.60